The Effects of High Fat Diet, Bone Healing, and BMP-2 Treatment on Endothelial Cell Growth and Function

Fazal Ur Rehman Bhatti[1,2Ψ], Ushashi C. Dadwal[1,2Ψ], Conner R. Valuch[3Ψ], Nikhil P. Tewari[1], Olatundun D. Awosanya[1], Caio de Andrade Staut[1], Seungyup Sun[1], Stephen K. Mendenhall[1], Anthony J. Perugini, III[1], Rohit U. Nagaraj[1], Hanisha L. Battina[1], Murad K. Nazzal[1], Rachel J. Blosser[1,2], Kevin A. Maupin[1], Paul J. Childress[1,2], Jiliang Li[3], Melissa A. Kacena[1,2]*

[1]Department of Orthopaedic Surgery, Indiana University School of Medicine, IN, USA

[2]Richard L. Roudebush VA Medical Center, IN, USA

[3]Department of Biology, Indiana University Purdue University Indianapolis, IN, USA

[Ψ]Contributed equally to this work

*Corresponding Author:
Melissa A. Kacena, Ph.D.
Director of Basic and Translational Research
Professor of Orthopaedic Surgery
Indiana University School of Medicine
1130 W. Michigan St, FH 115
Indianapolis, IN 46202
(317) 278-3482 – office
(317) 278-9568 – fax
mkacena@iupui.edu

This is the author's manuscript of the article published in final edited form as:

Bhatti, F. U. R., Dadwal, U. C., Valuch, C. R., Tewari, N. P., Awosanya, O. D., de Andrade Staut, C., Sun, S., Mendenhall, S. K., Perugini, A. J., Nagaraj, R. U., Battina, H. L., Nazzal, M. K., Blosser, R. J., Maupin, K. A., Childress, P. J., Li, J., & Kacena, M. A. (2021). The effects of high fat diet, bone healing, and BMP-2 treatment on endothelial cell growth and function. Bone, 146, 115883. https://doi.org/10.1016/j.bone.2021.115883

ABSTRACT

Angiogenesis is a vital process during the regeneration of bone tissue. The aim of this study was to investigate angiogenesis at the fracture site as well as at distal locations from obesity-induced type 2 diabetic mice that were treated with bone morphogenetic protein-2 (BMP-2, local administration at the time of surgery) to heal a femoral critical sized defect (CSD) or saline as a control. Mice were fed a high fat diet (HFD) to induce a type 2 diabetic-like phenotype while low fat diet (LFD) animals served as controls. Endothelial cells (ECs) were isolated from the lungs (LECs) and bone marrow (BMECs) 3 weeks post-surgery, and the fractured femurs were also examined. Our studies demonstrate that local administration of BMP-2 at the fracture site in a CSD model results in complete bone healing within 3 weeks for all HFD mice and 66.7% of LFD mice, whereas those treated with saline remain unhealed. At the fracture site, vessel parameters and adipocyte numbers were significantly increased in BMP-2 treated femurs, irrespective of diet. At distal sites, LEC and BMEC proliferation was not altered by diet or BMP-2 treatment. HFD increased the tube formation ability of both LECs and BMECs. Interestingly, BMP-2 treatment at the time of surgery reduced tube formation in LECs and humeri BMECs. However, migration of BMECs from HFD mice treated with BMP-2 was increased compared to BMECs from HFD mice treated with saline. BMP-2 treatment significantly increased the expression of CD31, FLT-1, and ANGPT2 in LECs and BMECs in LFD mice but reduced the expression of these same genes in HFD mice. To date, this is the first study that depicts the systemic influence of fracture surgery and local BMP-2 treatment on the proliferation and angiogenic potential of ECs derived from the bone marrow and lungs.

Keywords:

Angiogenesis; Endothelial cells; Bone; Type 2 diabetes; Fracture healing; Bone healing; Bone Regeneration; Bone morphogenetic protein; High fat diet

Abbreviations

BMECs, bone marrow endothelial cells; BMP-2, bone morphogenetic protein-2; BSA, bovine serum albumin; CSD, critical sized defect; DAPI, 4′,6-diamidino-2-phenylindole; GTT, glucose tolerance testing; HFD, high fat diet; HSC, hematopoietic stem cell; IM, intramedullary; i.p., intraperitoneal; ITT, insulin tolerance testing; LECs, lung endothelial cells; LFD, low fat diet; MSC, mesenchymal stem cell; NBF, neutral buffered formalin; PBS, phosphate buffered saline; T2D, type 2 diabetes mellitus; *Tie2CreERT*$^{+}$, *Tie2-CreER;Td-Tomato*; VEGF, vascular endothelial growth factor

1. Introduction

The prevalence of type 2 diabetes mellitus (T2D) increases with obesity and age [1]. T2D patients have an increased 1.4% relative risk of fracture compared to non-diabetic patients [2-6] and an increased risk of fragility fractures in the presence of coexisting osteoporosis [7]. Furthermore, the secondary manifestations of T2D, such as neuropathy, hypoglycemic episodes, retinopathy, and heart disease, all increase the risk of falls that cause traumatic fractures [6, 8, 9]. Once fractures occur, T2D-mediated complications lead to impaired bone healing and increased frequency of partial-, delayed-, or nonunion bone defects [10-12]. More specifically, an imbalance between osteoclasts and osteoblasts, local growth factors, mechanical stress, and impaired vasculogenesis prolongs the healing period by up to 87% [10, 13]. Thus, bone healing is dependent upon the synergistic actions of cells, cytokines, and growth factors. Various growth factors involved in bone regeneration have been identified and are already being used in clinical settings. For instance, bone morphogenetic protein-2 (BMP-2), a mediator of osteogenesis, and vascular endothelial growth factor (VEGF), a mediator of angiogenesis, are the most studied growth factors in this context [14, 15].

Angiogenesis can be regarded as a rate-limiting factor for appropriate bone repair [16, 17]. This process is vital for developing new bone tissue, remodeling, and maintaining homeostasis [18]. The formation of new blood vessels brings oxygen and nutrients to the highly metabolically active callus and also brings in inflammatory and precursor cells necessary for bone formation [19, 20]. The major components of angiogenesis include endothelial cell (EC) proliferation, migration, adhesion, and tube formation regulated by proangiogenic factors [21]. Although previous studies have shown organ/tissue-specific EC heterogeneity [22], EC heterogeneity between bones and lungs has not been reported. In this study, we examined ECs isolated from humeri bone marrow and compared them with ECs isolated from lungs, and also examined *in vivo* angiogenesis at the site of the bone fracture.

Secretion of VEGF from bone cells can trigger signaling responses in ECs to form blood vessels [23-25]. ECs residing in bone also release factors that can act upon chondrocytes and cells of the osteoblast lineage [26, 27]. For instance, ECs secrete

osteogenic factors, such as BMP-2, that support osteoblast differentiation [28]. ECs are also involved in the maintenance and differentiation of bone marrow hematopoietic stem cells (HSCs) [29]. Thus, angiogenesis plays a major role in the healing and repair of fractures [19, 30]. Indeed, altered vasculature is associated with the progression of numerous bone diseases, such as osteoporosis, osteonecrosis, rheumatoid arthritis, bone cancer, and metastasis [31].

Critical sized defect (CSD) models have been established to study nonunion and large bone defects, particularly those that do not heal during the lifetime of an animal [32]. The CSD model impedes fracture healing due to a lack of blood flow at the fracture site. This model allows researchers to study various aspects of fracture healing. The effect of BMP-2 on healing CSDs has been abundantly studied. However, to the best of our knowledge, there has not been a study that compares the systemic effects of local BMP-2 treatment in a murine CSD model on ECs. Therefore, in this study, we also investigated the effect of BMP-2 treatment in a CSD mouse model on the proliferation and angiogenic potential of ECs obtained from humeri bone marrow and lungs in HFD-induced type 2 diabetic mice three weeks post-surgery.

2. Materials and methods

2.1. Overview of experimental design and type 2 diabetic mouse model

Supplemental Fig. 1 is a timeline of our study design and Supplemental Fig. 2 shows the distribution of mice into our experimental groups. All animal studies were approved by the Indiana University School of Medicine Institutional Animal Care and Use Committee.

A total of fifty-five (n = 55) male *Tie2-CreER;Td-Tomato* (*Tie2CreERT*$^{+}$) mice were used in this study (Supplemental Fig. 2). The description of the original generation and characterization of these mice was previously reported [33]. The mice used in these studies have been backcrossed to the C57BL/6J background for more than 10 generations. At 6 weeks of age, the mice were placed on a low-fat diet (LFD) of Rodent Diet 10 kcal% fat (Research Diets, Inc., New Brunswick, NJ). Mice were assessed for total, lean, and fat body mass using an EchoMRI™-100H Body Composition Analyzer (EchoMRI, LLC, Houston, TX) and baseline glucose tolerance testing (GTT) at 7 weeks of age. At 8 weeks of age, baseline insulin tolerance testing (ITT) was completed. For GTT, mice were fasted for 6h and injected with glucose at a concentration of 2g/kg body weight. Blood was subsequently drawn from the tail vein, and glucose concentration was measured at 0-, 10-, 20-, 30, 60-, and 120-min. For ITT, mice were fasted for 2h, followed by Humulin R insulin (Eli Lilly, Indianapolis, IN) injection at 0.75 IU/kg body weight. Blood was drawn from the tail vein and glucose concentration measured at 15min intervals for 1h. Subsequently, the mice were split into two groups, with half remaining on LFD (n=27) and half switched to a high fat diet (HFD) (n=28) of Rodent Diet 45 kcal% fat (Research Diets, Inc., New Brunswick, NJ) (Supplemental Fig. 2). After 11 weeks on diet, mice were injected (intraperitoneal) with 10mg/kg tamoxifen for three consecutive days to induce *Cre-recombinase* and *Td-Tomato* expression in *Tie2*$^{+}$ ECs. Note that we first completed a pilot study which showed that administration of tamoxifen in this manner allows for Cre recombination but does not impact bone phenotype as assessed by µCT (Supplemental Figs. 3 and 4), whereas administration at 100mg/kg tamoxifen, while allowing for Cre recombination, increased some

trabecular and cortical bone parameters, thus our selection of 10mg/kg tamoxifen dosing.

After 12 weeks on diet, GTT/echoMRI was repeated (20 week old mice), and at 13 weeks (21 week old mice), ITT was repeated to confirm T2D phenotype. A week later, mice underwent CSD surgery as described below (22 week old mice). Therefore, mice remained on the respective diets for 14 weeks total prior to surgery.

2.2. Critical size defect (CSD) mouse model and BMP-2 treatment

All surgical procedures were performed under sterile conditions. The LFD and HFD animals were randomly sub-divided by cages into 2 groups based on treatment with either saline (Aqualite System, Hospira Inc, Lake Forest, IL) or recombinant human BMP-2 (Medtronic Sofamor Danek Inc, Memphis, TN) (Supplemental Fig. 2). Briefly, mice were anesthetized by isoflurane (Patterson Veterinary, Greeley, CO). Eyes were protected with Eye Lubricant Major® LubriFresh™ P.M. eye ointment (Major Pharmaceuticals, Indianapolis, IN). The right hind limb was shaved and disinfected with triplicate ethanol (Decon Laboratories, Inc, King of Prussia, PA) and Betadine (Purdue Products, LP, Stamford, CT) scrubs. To develop a CSD, a 1 cm skin incision was made laterally over the right thigh. The femur was exposed through blunt dissection and the knee was held in a flexed position to split the patellar tendon with the help of a 27-gauge needle. A 2 mm femoral diaphyseal defect was created with a sterile 200 Two Speed Rotary Tool (DREMEL, Racine, WI) and the needle was passed through a 2 mm synthetic graft and the greater trochanter [34]. The needle was secured in its position by bending inferiorly on itself and by pulling the needle taut against the greater trochanter in an anterograde direction. Either normal saline (negative control) or 5 µg recombinant human BMP-2 treated RCM6 Resorbable Collagen Membranes (ACE Surgical Supply Co., Inc., Brockton, MA) were wrapped around the synthetic graft and sutured into place using 3-0 polyglycolic acid suture (J215H, Ethicon, Somerville, NJ). The muscle fascia was closed using 3-0 polyglycolic acid suture and the skin was closed using standard 7 mm wound clips (RF7CS, Braintree Scientific, Braintree, MA). X-ray images were taken immediately after surgery and biweekly to ensure proper placement of the pin and

healing of the defects, respectively. Mice were euthanized three weeks post-surgery to isolate ECs and to examine *in vivo* vascularization and bone union.

2.3. Micro-computed tomography imaging and analysis of CSD bone union

For the tamoxifen dosing pilot study, femurs were imaged using a desktop SkyScan 1172 µCT imaging system (SkyScan, Kontich, Germany, 60 kV, 5.9 µm voxel), and image reconstructions of each specimen were obtained via NRecon v.1.7.3. For trabecular analysis of the femur, the ROI started at 0.25 mm proximal of the distal growth plate and extended an additional 0.5 mm proximally. Reported variables include BV/TV, Tb.Th, Tb.N, Tb.Sp, and Conn.D. For cortical analysis of the femur, a 1 mm ROI was centered on the midshaft of the femur. Reported variables include BV/TV, Cortical T.Ar, Cortical B.Ar, Cortical M.Ar, Cortical MMI Polar, and Cortical Thickness.

For the CSD femur imaging, a desktop SCANCO µCT35 imaging system (SCANCO Medical, Brüttisellen, Switzerland, 55 kV, 12 µm voxel) was used. For fracture callus analysis, the ROI was centered at the midpoint of the scaffold and extended until the callus ended in each direction.

Bone union was quantitated using the Radiographic Union Score for Tibial Fractures (RUST) method [35] but was adapted and applied to the femora [36, 37] as a semi-quantitative method for analysis. Here, orthogonal images were selected, which approximated the medial, lateral, anterior, and posterior cortices on the 3D reconstructions of the callus region in the femur. Then, each cortex was given a score of 1 (callus absent), 2 (callus present, incomplete bridging), or 3 (callus present, complete bridging). The scores for all 4 cortices were added to provide a final score ranging from 4 (not healed) to 12 (maximally healed). Supplemental Fig. 5 contains annotated µCT images depicting this scoring system.

2.4. Histological imaging and analysis of vasculature within the defect region

Both the fractured femurs and the contralateral femurs were collected 3 weeks after the fracture surgery. All the femurs were fixed in 10% neutral buffered formalin (NBF, Thermo Fisher Scientific, Waltham, MA) for 48 hours, transferred to 70% ethanol, and stored at 4°C. Following µCT scanning, femurs were demineralized in Immunocal

Decalcifier (Statlab, Mckinney, TX) for 48 hours at 4°C. The femurs were then processed and embedded in paraffin. 5-µm thick longitudinal sections were cut and mounted on glass slides. Some sections were stained with Alcian Blue/Picrosirius Red to better visualize the fracture site and cartilage area as described elsewhere [38].

Other sections were deparaffinized, treated with 3% H_2O_2 to inhibit endogenous peroxidase activity, and blocked with 3% bovine serum albumin (BSA, Sigma-Aldrich, St. Louis, MO). Antigen retrieval was performed with 10mM citrate buffer for 20 minutes. Samples were incubated with 1:100 dilution of Rat monoclonal anti-Endomucin antibody (SC-65495, Santa Cruz Biotechnology, Santa Cruz, CA) in blocking buffer at 4°C overnight. Following three washes in 1X PBS, sections were incubated with 1:200 dilution of biotinylated anti-rat IgG secondary antibody, and color was developed with a diaminobenzidine substrate chromogen system (VectaStain ABC kit, Vector Laboratories, Burlingame, CA). Non-immune IgD was used as a negative control. A 0.2% methyl green solution was used as a counterstain. Vessel area and perimeter were measured and vessel number was counted in the periosteal callus area using a semiautomatic analysis system (Bioquant OSTEO, Bioquant Image Analysis Co., Nashville, TN) attached to a Leica microscope. The measurements were carried out at upper and lower bony callus regions above and below the scaffold (Supplemental Fig. 6 depicts the regions from which micrographs were obtained). Vessel number, area, and perimeter were calculated for each region and presented as the average of those 3 regions per callus area. Adipocytes were counted in the same regions and were presented as the average number of adipoctyes per microscopic field.

2.5. Isolation of endothelial cells from lungs and bone marrow

ECs were isolated from lungs (LECs) and bone marrow (BMECs) as described previously with slight modifications [39, 40]. Briefly, lung tissue was isolated and harvested in a sterile environment, finely minced into small pieces, and then digested with 225 U/ml collagenase type 2 solution (Worthington Biochemical Corporation, Lakewood, NJ) for 1 h at 37°C and 5% CO_2. Simultaneously, Dynabeads (Thermo Fisher Scientific) were conjugated with biotin rat anti-mouse CD31 antibody (BD Pharmingen™, San Jose, CA). The minced tissue was filtered through a 70 µm mesh

strainer and the cell suspension was incubated with the CD31-conjugated Dynabeads for 1h at 4°C. Later, $CD31^+$ cells were separated by magnetic field using a Dynamag 2 (Thermo Fisher Scientific). Isolated cells were plated in collagen I coated 6-well plates (Corning®, Corning, NY) at a density of 3 x 10^5 cells/ml in EC Growth Medium 2 (PromoCell, Heidelberg, Germany) supplemented with Growth Medium 2 SupplementMix (PromoCell) and Penicillin-Streptomycin-Glutamine (Thermo Fisher Scientific). LECs at passage 2 were used in all experiments.

BMECs were isolated from the humeri. Briefly, soft tissues were removed thoroughly, epiphyses were removed, and the bone marrow was isolated by centrifugation in Complete EC Growth Media supplemented with 5% fetal bovine serum (FBS), EC Growth Supplement, and 1% Penicillin/Streptomycin (ScienCell, Carlsbad, CA). Isolated ECs were plated in a 12-well plate coated with 4 µg/mL fibronectin (Thermo Fisher Scientific) in Complete EC Growth Media and were used after 7 days in culture.

Of note, from a feasibility perspective, 3-4 mice/group were euthanized at any particular time. This was repeated 3-4 times to obtain sufficient cell numbers for all assays and technical replicates for each biological replicate (individual mice for BMECs and pooled mice for LECs).

2.6. Immunofluorescence for CD31 expression

Cultured LECs and BMECs at 70-80% confluence were fixed with 10% NBF, washed with 1X phosphate buffered saline (PBS) (IBI Scientific, Cubuque, IA), and stained overnight with anti-CD31/PECAM-1, DyLight 488, Clone: MEC 7.46, antibody (Novus Biologicals™, Centennial, CO) at 4°C at a dilution of 1:500 in 1% BSA. Nuclei were stained with 1 µg/ml 4′,6-diamidino-2-phenylindole (DAPI) solution (Thermo Fisher Scientific). The images were taken with EVOS® FL Cell Imaging System (Thermo Fisher Scientific).

2.7. Analysis of proliferation

The proliferation of LECs was assessed by seeding cells in a 24-well plate at a density of 5x10^3 cells/well. Cells were fixed with 10% NBF and staining the nuclei with 1

µg/ml DAPI solution. The images were taken with EVOS® FL Cell Imaging System and DAPI positive cells were counted manually.

The proliferation of BMECs was examined by seeding the cells in a 96-well plate at a density of $5x10^3$ cells/well. Cells were fixed with 10% NBF at room temperature for 20 min, then stained with 0.05% crystal violet for 30 min. Later, cells were washed under tap water and dried overnight. The images were taken with EVOS® FL Cell Imaging System and counted using ImageJ.1.52a software [41].

2.8. Tube formation assay

Tube formation was assessed by Matrigel tube formation assay as described previously [42]. Briefly, Matrigel basement membrane matrix (Corning®, Corning, NY) was polymerized in 96-well plates (50 µl/well) at 37°C for 45 minutes. LECs at passage 2 and BMECs at passage 1 were plated on the polymerized basement membrane matrix at a density of 10,000 cells/well suspended in their respective growth medium. Cells were incubated at 37°C and 5% CO_2, and images were taken after 6h and 8h for lung and bone marrow cells, respectively. Tube formation was quantified using ImageJ.1.52a software. The parameters analyzed for tube formation included the number of nodes, number of meshes, number of complete tubes, and total tube length. The number of nodes and the number of meshes were analyzed by the automated Angiogenesis Analyzer plugin using ImageJ.1.52a. The number of complete tubes and the total tube length were measured manually by three independent double-blinded readers using the Simple Neurite Tracer plugin within the ImageJ.1.52b Fiji software [43]. Supplemental Figure 7 shows a representative Matrigel tube formation micrograph with annotations showing the measured parameters.

2.9. Wound migration assay for BMECs

BMECs were seeded in 96 well plates at a density of 1×10^5 cells/well and grown for 24 h until 100% confluence. A wound was created in the middle of each well using IncuCyte® WoundMaker (Essen BioScience, Ann Arbor, MI). Images were taken at time 0 and consecutively every 2h until 48h at 10X magnification using the IncuCyte ZOOM® Live-Cell Analysis System (Essen BioScience). Images were analyzed using the

IncuCyte™ Scratch Wound Cell Migration Software (Essen BioScience). The parameters for migration assessed were relative wound density (%), wound confluence (%), and wound width (µm).

2.10. Gene expression analysis

RNA was isolated from the cells using an RNeasy Mini kit (QIAGEN, Hilden, Germany). The Transcriptor First Strand cDNA Synthesis Kit (Roche, Basel, Switzerland) was used to prepare cDNA from 1 µg of total RNA. Quantitative real-time PCR was performed using Power SYBR™ Green PCR Master Mix (Thermo Fisher Scientific, Waltham, MA) on a CFX96 Touch Real-Time PCR Detection System (Bio-Rad, Hercules, CA). The following primer genes were analyzed: CD31 Antigen (CD31), Fms Related Tyrosine Kinase 1 (FLT-1), Angiopoietin 1 (ANGPT1), and Angiopoietin 2 (ANGPT2) (Table 1). Glyceraldehyde-3-Phosphate Dehydrogenase (GAPDH) gene served as the internal control. Relative gene expression was calculated using the $2^{-\Delta\Delta CT}$ method.

Table 1

Quantitative PCR primers used in the study

Gene	Orientation	Sequence (5′-3′)
GAPDH	Forward	CGTGGGGCTGCCCAGAACAT
	Reverse	TCTCCAGGCGGCACGTCAGA
CD31	Forward	ACGCTGGTGCTCTATGCAAG
	Reverse	TCAGTTGCTGCCCATTCATCA
FLT-1	Forward	CCACCTCTCTATCCGCTGG
	Reverse	ACCAATGTGCTAACCGTCTTATT
ANGPT1	Forward	CACATAGGGTGCAGCAACCA
	Reverse	CGTCGTGTTCTGGAAGAATGA
ANGPT2	Forward	CCTCGACTACGACGACTCAGT
	Reverse	TCTGCACCACATTCTGTTGGA

2.11. Statistical analysis

Statistical analyses were performed using GraphPad Prism version 8.0.0 for Windows (GraphPad Software, San Diego, California USA, www.graphpad.com). ANOVA followed by Bonferroni's post-hoc multiple-comparisons test was completed to evaluate the significance of differences found between all groups when there were more than two present, whereas a Student's t-test was performed to evaluate the significance of a difference found between two groups. Three-way ANOVA was performed to analyze the migration data. Statistically significant differences were those where $p \leq 0.05$. Unless otherwise specified, the data are presented as the mean ± standard deviation (SD). All experiments were conducted with 3 or more biological replicates (as detailed in each figure/legend), and triplicate or quadruplicate wells or technical replicates were averaged for each biological replicate.

3. Results

3.1. HFD resulted in T2D-like phenotype in mice

Mice fed with HFD for a 12-week time period developed a T2D-like phenotype (Fig. 1). HFD fed mice gained a considerable amount of weight over time irrespective of treatment (Fig. 1A). Blood glucose levels were recorded for a total of 41 animals when they were 7 and 8 weeks of age for baseline GTT and ITT tests, respectively, and were repeated at the 20 and 21 weeks of age, respectively. It was evident that HFD resulted in impaired glucose and insulin tolerance in mice (Fig. 1B and C and Supplemental Fig. 8). Moreover, HFD mice had a significantly higher total body mass compared to LFD mice (Fig. 1D). A slight difference was observed in the lean mass of HFD mice (Fig. 1E). The fat mass was considerably higher in HFD fed mice (Fig. 1F). These data show that HFD induced a T2D-like phenotype in mice.

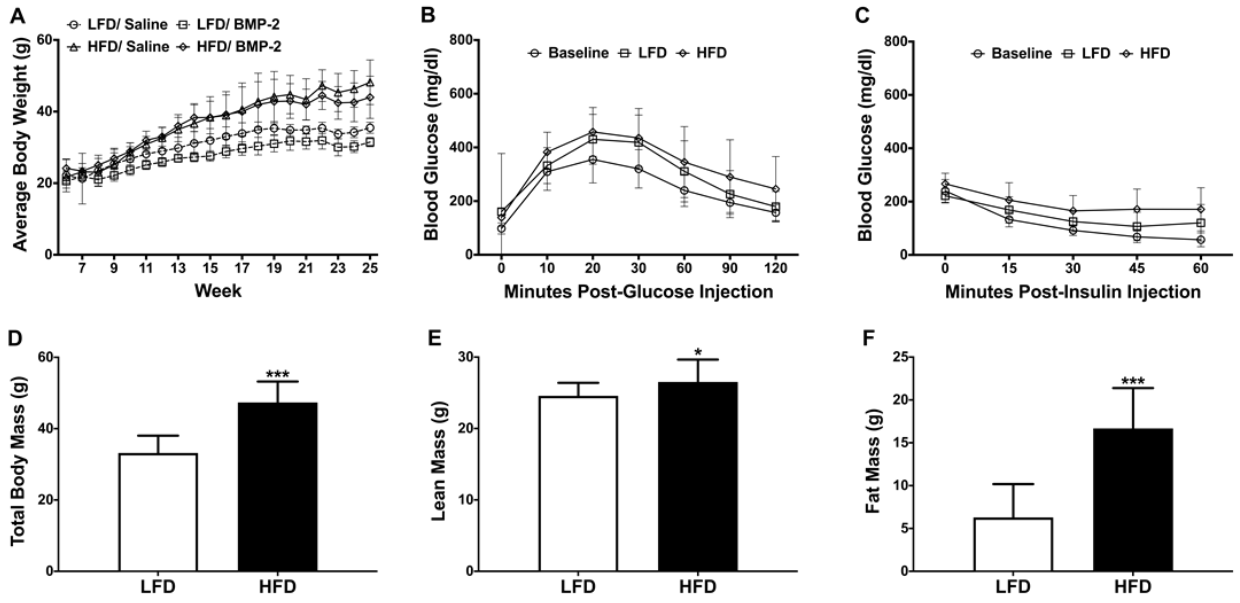

Fig. 1. T2D-like phenotype induced in mice fed with HFD. Average body weight of 27 LFD and 28 HFD fed mice over the course of 25 weeks (A). GTT data showing average blood glucose levels of 20 LFD and 21 HFD fed mice after being on the diet for 12 weeks compared to the average baseline blood glucose level. The baseline is a combined total of 41 mice measured when they were 7 weeks of age (B). ITT data showing average blood glucose levels of 20 LFD and 21 HFD fed mice after being on diet for 12 weeks as compared to the average baseline blood glucose level. The baseline is a combined total of 41 mice measured at 8 weeks of age (C). Total body mass (D), lean mass (E), and fat mass (F) of LFD and HFD fed mice. Data are expressed as mean ± SD. *$p < 0.05$ and ***$p < 0.001$ as compared to LFD mice.

3.2. CSD healing in diabetic mice 3 weeks post-surgery

Bone healing was examined 3 weeks post-surgery for mice fed a LFD or HFD and treated locally at the time of surgery with either saline or BMP-2. This is the same time that LECs and BMECs were isolated from the mice for *in vitro* studies detailed below. Fig. 2 shows representative µCT reconstructions of the injured femurs from these mice and Fig. 3 shows the quantitated µCT data obtained as well as RUST scoring as a measure of bone union. As detailed in Fig. 2 and Fig. 3E, irrespective of diet, bridging

was not observed in any of the saline treated mice. Specifically, the LFD+Saline group had a RUST score of 5.0 ± 0.9 and the HFD+Saline group had a RUST score of 5.9 ± 2.7 ($p>0.05$). On the other hand, BMP-2 treatment increased bone union/bridging in both LFD (RUST: 9.0 ± 3.6) and HFD (RUST: 11.1 ± 1.8) mice ($p=0.05$). With regard to µCT parameters, mineralized callus volume (BV/TV) and trabecular number (Tb.N) followed similar trends. Of importance, as detailed in Fig. 2, 3 of 9 (1/3) of LFD mice treated with BMP-2 had not completely healed by 3 weeks post-surgery. Thus, we also separated healed and unhealed specimens for additional analysis of the µCT data and RUST scoring data (Supplemental Fig. 9). When LFD+BMP-2 mice that healed were compared with HFD+BMP-2 mice, no significant differences in any parameters were observed ($p > 0.05$). Thus, it appears that in a femoral CSD model, that BMP-2 improves bone healing, irrespective of diet.

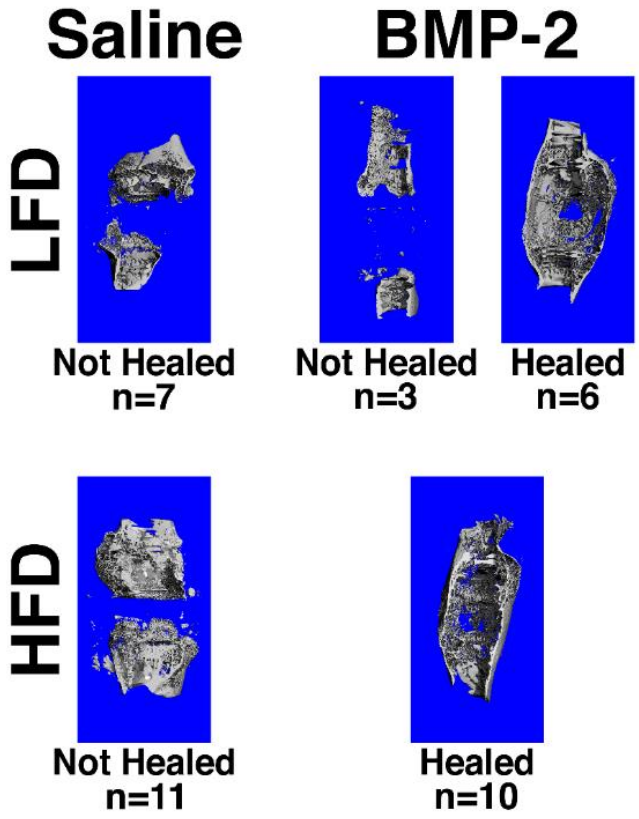

Fig. 2. Representative µCT reconstructions from mice that underwent a femoral CSD surgery, were treated locally at the time of surgery with either saline or BMP-2, and were fed either a HFD or LFD. Below each image, the n-value represents the number of

mice in each group that were considered healed (average of 3 or more cortices receiving a score of 3, RUST ≥ 10) or not healed (average of 2 or more cortices receiving a score of 1, RUST ≤ 6).

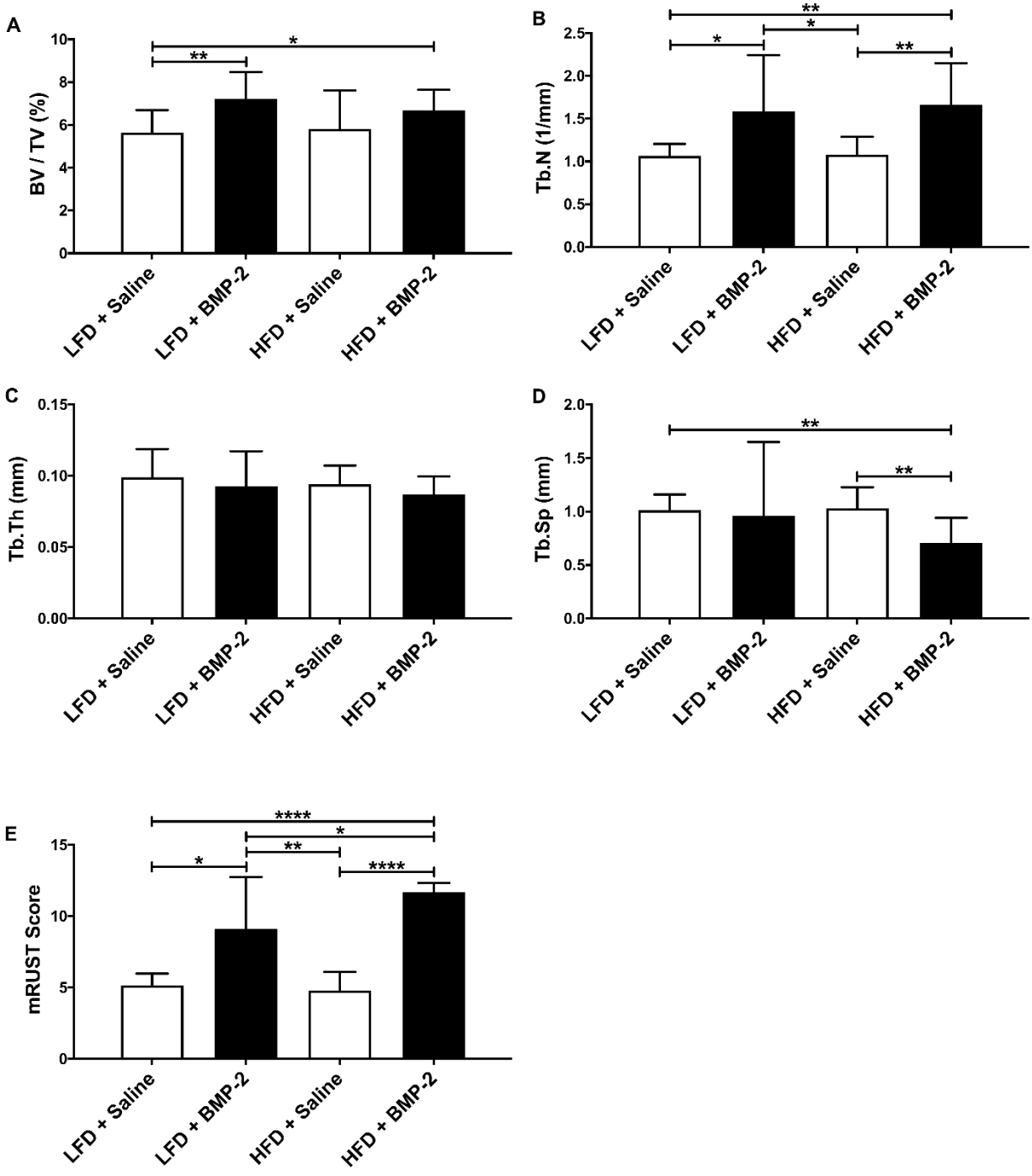

Fig. 3. Reconstructed µCT images were analyzed and several parameters were examined within the fracture callus region, including: mineralized callus volume (BV/TV) (A), trabecular number (Tb.N) (B), trabecular thickness (Tb.Th) (C), trabecular separation (Tb.Sp) (D), and RUST scoring (E) for each group. For RUST scoring, each cortex of the fracture callus as observed on the reconstructed images (orthogonal views) were given a score of 1 (callus absent), 2 (callus present, incomplete bridging), or 3 (callus present, complete bridging), and the scores for all 4 cortices were combined to provide a final score ranging from 4 (not healed) to 12 (maximally healed). Data are expressed as mean ± SD (n=7-11/group). *$p \leq 0.05$, **$p \leq 0.01$, ***$p \leq 0.001$, and ****$p \leq 0.0001$.

3.4. Histological analysis at the fracture site

Following µCT analysis, femurs were decalcified, paraffin-embedded, and sectioned. To confirm the bone union/bridging observed in mice treated with BMP-2, some sections were stained with Alcian Blue/Picrosirius Red as per published protocols [38]. Representative images from each group are shown in Supplemental Fig. 10. Other sections underwent immunohistochemical staining for endomucin and were subsequently quantitated (Fig. 4 and Supplemental Fig. 11). As would be expected when examining the fracture callus, in the saline treated mice, where complete bridging did not occur, there is reduced callus for which vessel parameters can be measured (no vessels are present in the middle callus section (section #2) described in Supplemental Fig. 6). Therefore, these vessel parameters were overall lower in saline treated mice as compared to that observed in BMP-2 treated mice. No significant differences were observed based on diet.

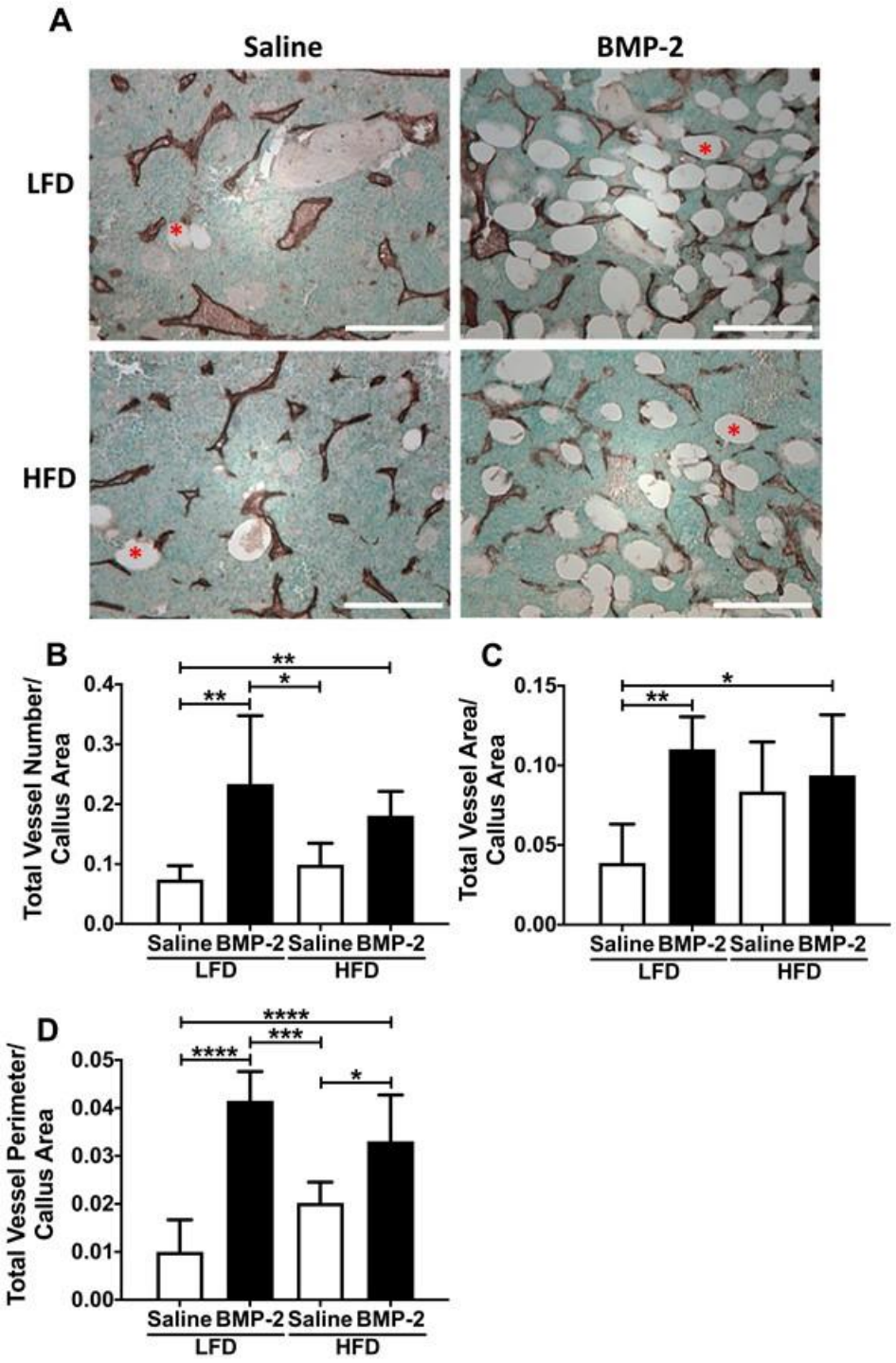

Fig. 4. Representative microscopic images showing microvascular vessels inside bony callus as indicated by ECs immunostained with endomucin (dark brown) three weeks after fracture surgery (A). Adipocytes (*) were also observed. Original magnification = 20X, Scale bar = 100 µm. The total vessel number/callus area (B), total vessel

area/callus area (C), and total vessel perimeter/callus area (D) were measured. Data are expressed as mean ± SD (n=5-7/group). *$p \leq 0.05$, **$p \leq 0.01$, ***$p \leq 0.001$, and ****$p \leq 0.0001$.

As we were interested in understanding whether local administration of BMP-2 at the fracture site could impact vessel formation at distal sites, we also examined endomucin stained vessels within the bone marrow at the midshaft of the contralateral limb from all of these mice. As shown in Supplemental Fig. 12, virtually no differences were observed in any of the vessel parameters measured in contralateral limbs based on diet or based on treatment.

While our goal was to examine vessel parameters, we observed (Fig. 4A) that BMP-2 treated mice, irrespective of diet, had significantly more adipocytes in the callus area (Supplemental Fig. 13), but not in the contralateral bone marrow area (data not shown).

3.5. Characterization of ECs in vitro and induction of TdTomato expression

In order to examine the systemic effect of bone healing on ECs, ECs were isolated 3 weeks after surgery. LECs exhibited typical EC morphology in culture (Supplemental Fig. 13A). Tamoxifen injections (10mg/kg) resulted in the induction of *TdTomato* expression in LECs that express *Tie2*-specific *Cre* recombinase (Supplemental Fig. 4 and 14B). Furthermore, the LECs used in this study expressed characteristic CD31 markers on the surface of the cell membrane (Supplemental Fig. 14D&F). The LECs retained *TdTomato* expression following the formation of tubes (Supplemental Fig. 13G-H). Thus, LECs used in this study were characterized based on surface expression of CD31, induced expression of *TdTomato*, and/or functional ability to form tube-like structures on the Matrigel matrix.

The BMEC isolation initially provides a more heterogenous cell population than that of the CD31 separated LECs. However, this method has been validated by several groups via flow cytometric analysis [44] and immunocytochemistry [45] and has also

been compared to other EC cell lines [46]. Specifically, this method reproducibly results in a high percentage of CD31+ cells that are able to form tube-like structures on Matrigel, a hallmark of ECs. Here we validate these findings qualitatively, showing in Supplemental Fig. 15B that 3 daily injections of 10 mg/kg of tamoxifen resulted in *TdTomato* expression in BMECs that express *Tie2*-specific *Cre* recombinase. In Supplemental Fig. 15, we also observe their ability to form tubes (C) and their expression of CD31 (D&F). Finally, in Supplemental Fig. 15G we present representative flow cytometry data showing that 63% of CD45-Ter119-TdTomato+ (Tie2+) cells are CD31+CD105+ ECs.

3.6. Proliferation of ECs isolated from lungs and bone marrow

Irrespective of diet or treatment, no significant differences were observed in the proliferation of ECs isolated from lungs or humeri (Fig. 5).

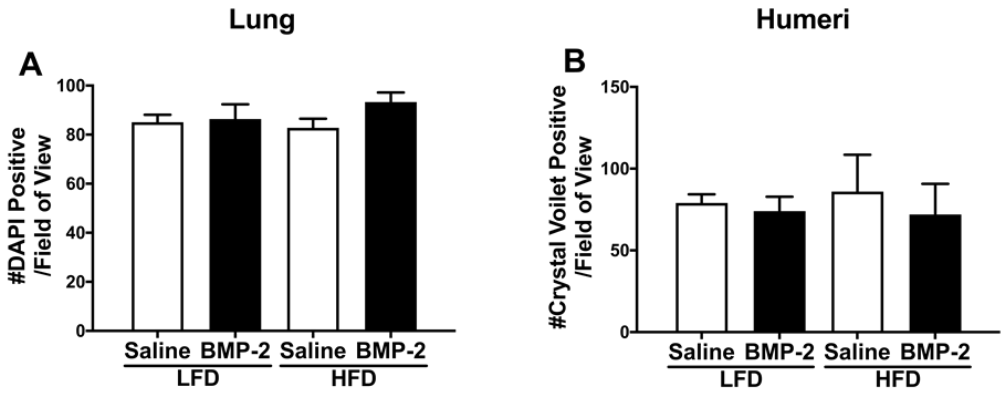

Fig. 5. Proliferation of ECs isolated from lungs (A) or humeri bone marrow (B). Data are expressed as the mean ± SD (n=3-4 biological replicates/group). No significant differences were detected.

3.7. Angiogenesis of EC in vitro

Angiogenic potential of ECs was evaluated by tube formation (Fig. 6). Tube formation was assessed by numbers of nodes, meshes, and tubes, as well as total tube

length. LECs showed enhanced angiogenic potential in the HFD group as compared to the LFD group (Fig. 6 A,C,E,G). In terms of treatment, irrespective of the diet, the LECs isolated from saline treated mice formed significantly more nodes, tubes, and total tube length as compared to LECs isolated from diet-matched BMP-2 treated mice. BMECs isolated from humeri showed a similar tube formation pattern as LECs (Fig 6 B,D,F,H). Specifically, the humeri BMECs isolated from the HFD, saline treated group showed the highest angiogenic potential followed by those isolated from the HFD, BMP-2 treated mice. In LFD mice, treatment of humeri BMECs with BMP-2 resulted in no difference in the number of nodes and the number of tubes, but resulted in a significant decrease in the number of meshes and total tube length. Overall, the tube formation data suggested that angiogenesis of LECs and BMECs was enhanced by HFD, but was reduced with *in vivo* BMP-2 treatment.

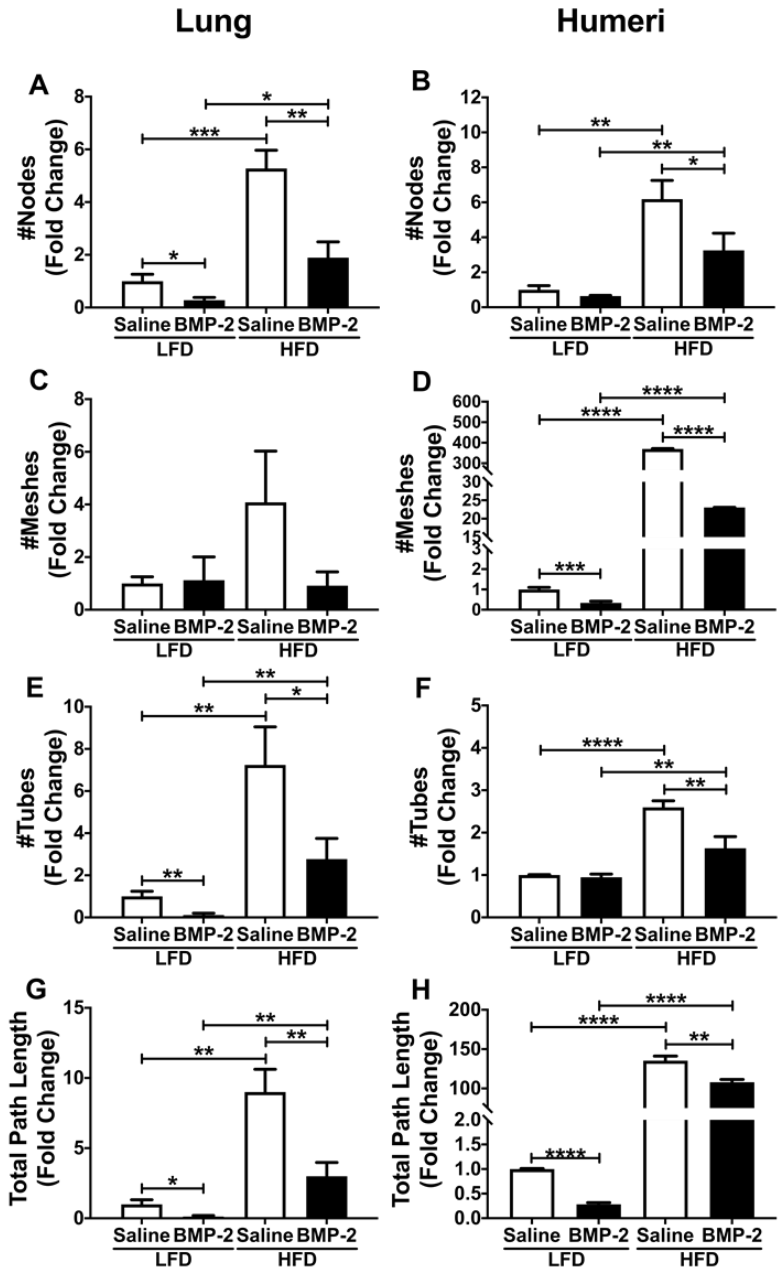

Fig. 6. Angiogenesis parameters associated with ECs isolated from the lung (A, C, E, G) or humeri bone marrow (B, D, F, H). The number of nodes (A, B), the number of meshes (C, D), the number of tubes (E, F), and the total path length (G, H) were quantified. Data are expressed as the mean ± SD (n=3-4 biological replicates/group). *$p \leq 0.05$, **$p \leq 0.01$, ***$p \leq 0.001$, and ****$p \leq 0.0001$.

3.8. Effect of migration in BMECs

Migration was evaluated in BMECs to examine the effect of HFD and BMP-2 treatment at the systemic level. Graphical results are shown for relative wound density (Fig. 7A), wound confluence (Fig. 7B), and wound width (Fig. 7C). 3-way ANOVA results for humeri BMECs showed significant effects in all 3 migration parameters by time, diet, and treatment, as well as a diet by treatment effect. Most notably, the HFD mice treated with BMP-2 showed significant increases in relative wound density and decreases in wound width.

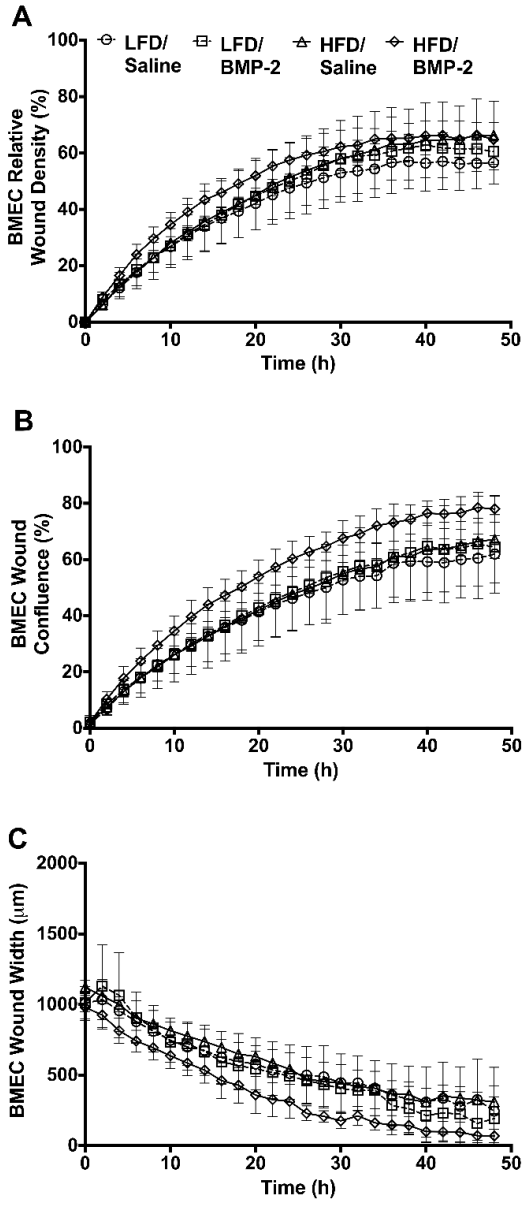

Fig. 7. Migration of ECs isolated from humeri bone marrow. The relative wound density (A), wound confluence (B), and wound width (C) were determined. The graphs represent data collected for all the groups every 2h for 48h. Data are expressed as the mean ± SD (n=3-4 biological replicates/group).

3.9. Gene expression analysis of ECs

mRNA expression of CD31, FLT-1, ANGPT1, and ANGPT2 were examined in ECs isolated from lungs and humeri (Fig. 8). In the LFD group, saline versus BMP-2 treatment of LECs did not alter the expression of CD31 and ANGPT1 genes. However, in the LFD LECs, BMP-2 treatment significantly increased the expression of FLT-1 and ANGPT2 compared to saline treatment. In the HFD LECs, BMP-2 significantly decreased the expression level of CD31, FLT-1, ANGPT1, and ANGPT2 compared to that observed in the saline treated group. With regard to humeri BMECs, in the LFD group, BMP-2 significantly increased the expression of CD31, FLT-1, ANGPT1, and ANGPT2. On the other hand, in the HFD BMEC group, BMP-2 significantly reduced the expression of CD31, FLT-1, and ANGPT2, but no difference was seen for ANGPT1 expression. Interestingly, as observed with the tube formation assays, the general expression trends for CD31, FLT-1, and ANGPT2 were similar for humeri BMECs and LECs.

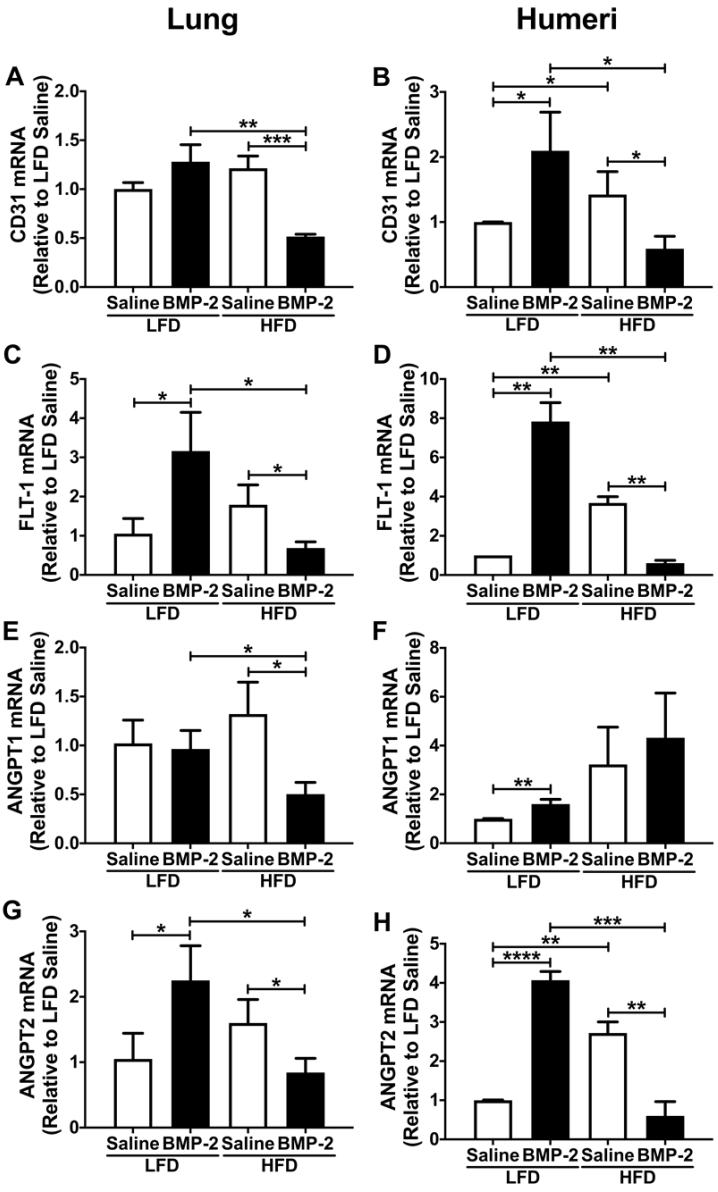

Fig. 8. Real-time PCR analysis of ECs isolated from the lungs (A, C, E, G) or humeri bone marrow (B, D, F, H). Relative mRNA expression was measured and calculated for the following genes: CD31 (A, B), FLT-1 (C, D), ANGPT-1 (E, F), and ANGPT-2 (G, H). LFD saline control expression was set to 1.0 and expression in all other samples are shown relative to the LFD saline control. Data are expressed as mean ± SD (n=3-4 biological replicates/group). Note the error on (D) is small and falls within the bolded outline of the bar. *$p \leq 0.05$, **$p \leq 0.01$, ***$p \leq 0.001$, and ****$p \leq 0.0001$. Data are expressed as the mean ± SD.

4. Discussion

Numerous studies have shown that persons with either type 1 diabetes (T1D) or T2D are at higher risk of fracture compared to the general population [11, 47, 48]. There are some distinct differences between persons with T1D and T2D with respect to their bone properties. Individuals with T1D tend to have a lower bone mineral density (BMD) than the general population, and their risk of fracture is significantly greater than the increased risk of fracture observed in individuals with T2D [11]. On the other hand, persons with T2D have a higher BMD than the general population. Yet, even with a higher BMD they have a higher risk of fracture, especially in the hip, compared to the general population [2]. Indeed, reports of up to a 69% increase in fracture risk compared to persons without T2D have been documented [49]. This discrepancy between BMD and fracture risk for persons with T2D suggests that properties other than bone quantity, such as bone quality as well as peripheral nerve, kidney, and vascular function, are critically important when examining fracture risk [48, 50, 51]. The latter, vascular function, is a primary focus of this study.

Although it should be noted that a few reports have shown either reduced fracture risk or no difference in fracture risk between individuals having T2D and the general population [52, 53], the majority of studies identify that T2D is a risk factor for fracture despite higher BMD. In fact, the World Health Organization's fracture assessment tool (FRAX) was shown to underestimate the fracture risk of persons with T2D, and therefore, diabetes is being considered as a risk factor for inclusion in future FRAX iterations [54].

Regardless of the magnitude of increased fracture in persons with T2D, impaired fracture healing is an established sequela of the disease. Indeed, one study examining ankle fractures indicated the rate of nonunion/delayed union to be 43% in persons with diabetes vs. 16% in persons without diabetes [55]. Clinical studies have shown that diabetic patients have impaired bone healing in long bones, the hip, and even the mandible [48, 51, 56, 57]. Another study showed that persons with either T1D or T2D were more likely to have fracture-healing complications (malunion, nonunion, delayed union) and suggested that the micro and macro-vascular disease associated with

diabetes may be responsible for the increased risk of fracture healing complications [58]. In the same vein, well-known complications of T2D include: diabetic retinopathy, foot ulcers, neuropathy, and delayed wound healing, all of which share compromised micro- and macrovascular performance as part of their pathophysiology [48, 50, 51].

Graves et al. [51] summarized the known changes observed in diabetic fracture healing at the tissue level: reduced bone formation, cartilage formation, and vascularity/angiogenesis. At the molecular level, the primary change was reduced growth factor expression. It is this combination of findings that led us to undertake a comprehensive examination of the impacts of HFD and local delivery of BMP-2 on bone healing and angiogenesis at the fracture site, as well as at distal locations (lung and humeri).

To accomplish this, we first needed to validate that our HFD model would result in a T2D-like phenotype. Here, mice were fed a HFD for 12 weeks and developed a T2D-like phenotype as expected (Fig. 1) [59]. Specifically, HFD animals gained significantly more weight compared to LFD animals. The T2D-like metabolic profile of HFD-fed mice was further confirmed by GTT and ITT [60]. Since the T2D-like mouse model used in this study is based on the induction of obesity, we observed increases in total body-, lean-, and fat-mass in HFD mice as compared to LFD mice [61]. These observations established that the HFD mice exhibited a T2D-like phenotype prior to surgery.

BMP-2 belongs to the transforming growth factor-β (TGF-β) superfamily of proteins and acts as a disulfide-link homodimer. BMP-2 regulates vital steps in the bone induction cascade such as mitosis, chemotaxis, and differentiation of mesenchymal stem cells (MSCs) during bone healing [62, 63]. BMP-2 also induces bone formation in CSDs [64]. Therefore, BMP-2 has served as a substitute to autografts for nonunion of bone defects, spinal fusion, fracture healing, and open tibial fractures [65, 66]. The European Medicines Agency (EMA) approved recombinant human BMP-2 (rhBMP-2) (InductOs®) for the treatment of single-level lumbar spine fusion and acute tibial fractures [67]. The U.S. Food and Drug Administration (FDA) approved rhBMP-2 (INFUSE® Bone Graft Device) for the treatment of open tibial fractures after stabilization with intramedullary nail (IM) fixation [67]. Like others [68, 69], in our

previous studies, we demonstrated that BMP-2 delivered locally at the time of surgery can robustly heal a rat femoral CSD [42]. Here, we observed that BMP-2 administration locally at the time of surgery resulted in bridging, robust callus formation, and union of fracture in all 10 HFD mice and 6 of 9 LFD mice 3 weeks post-surgery (Fig. 2 and Fig. 3E). At first glance, this finding seems somewhat counterintuitive to data suggesting that patients with T2D have impaired fracture healing. However, when considering that weight-bearing improves fracture healing [36, 70, 71] and that BMP-2 signaling is responsive to mechanical loading [72], it is understandable that fracture healing could be improved in mice with a higher body weight as they would exert more loading on the surgical limb.

To our knowledge, this is the first report where animal fracture healing with BMP-2 treatment is being studied in the context of HFD. Additionally, there have been only a small number of rodent investigations published using a HFD model. Chronologically, in 2012, Pirih et al [73], provided C57BL/6 male mice with a 37 kcal% HFD for 13 weeks. They created 3 mm cranial defects and investigated bone repair 5 weeks post-surgery. They observed a > 50% reduction in the bone volume fraction (BV/TV) and the bone surface/tissue volume (BS/TV) in HFD mice. In 2014, Brown et al. [74] provided C57BL/6 male mice with a 60 kcal% HFD for 12 weeks. They created open tibial fractures by using a scalpel blade and an intramedullary (IM) pin for stabilization. Mice on the HFD experienced significantly impaired bone healing in their model. Specifically, they observed a significant decrease in woven bone (up to 30% reduction), callus bone volume (up to 50% reduction), and torsional rigidity (up to a 28% reduction). Of importance, they also found a 44% reduction in vascular volume within the fracture callus in HFD mice. While this finding did not reach statistical significance, this observation highly suggests that impairments in vasculature may be part of the pathology observed at the site of healing in mice on HFD. More recently, Histing et al. [75] also provided C57BL/6 male mice with a 60 kcal% HFD, but for 20 weeks prior to creating closed femur fractures (3-point bending with IM pin stabilization). Femurs were examined 2 and 4 weeks post-surgery. In this study, no significant differences were reported with respect to fracture healing, which conflicts with the previous reports in the literature but is consistent with our findings in the saline treated mice. Indeed, as shown

in Fig. 3, no significant differences were observed between LFD and HFD, saline treated mice, 3 weeks post-surgery. While different mouse strains, bones, or methods of creating the fracture could certainly impact differences, it could also be the earlier time points with which both our data and Histing's data [75] were collected. Ongoing investigations in our laboratory will address whether differences are observed with longer follow-up post-surgery.

Angiogenesis is vital for bone repair and ECs play a significant role during angiogenesis [16, 17]. Therefore, our main goal was to determine the effect of HFD and BMP-2 treatment *in vivo* on ECs. Moreover, we asked whether the angiogenic potential of ECs would be different if isolated from different tissues, such as lung and bone marrow. With respect to angiogenesis at the fracture site, decalcified fractured femurs were stained for endomucin (Fig. 4A). As shown in Fig. 4 and Supplemental Fig. 11, BMP-2 treatment, along with enhancing bone healing, resulted in higher vessel parameters than did saline treatment, irrespective of diet. Thus, it appears that 3 weeks post-surgery, in a CSD model, angiogenesis at the fracture site appears unchanged based on diet but is robustly elevated based on BMP-2 treatment. Of note, the contralateral femur was also examined following endomucin staining and virtually no differences in vessel parameters were observed between groups (Supplemental Fig. 12).

Although BMP-2 is well known for its ability to stimulate differentiation of MSCs along the osteogenic pathway [76], here we see not only increases in bone formation but also an unexpected, robust upregulation in adipocytes within the fracture callus of BMP-2 treated mice irrespective of diet (Supplemental Fig. 13). While further studies are required to better understand this observation, it is possible that BMP-2 is acting to stimulate the *in vivo* proliferation of MSCs in general or bipotential osteo-/adipo-progenitor cells in particular. This idea is also consistent with research showing that BMP-2 treatment can increase adipogenesis in the presence of dexamethasone [77]. Whether the increase in adipogenesis within the fracture callus persists as time post-fracture increases remains to be determined, but it is something important to

understand due to the use of BMP-2 for several bone regeneration indications in humans.

As mentioned above, we were interested in not only examining angiogenesis at the fracture site but also at distal sites. With respect to the latter, ECs were isolated from the lungs and humeri of HFD and LFD mice treated with either saline or BMP-2 following a CSD surgery, were investigated for their proliferation, angiogenic potential, migration (or wound closure), and gene expression *in vitro* 3 weeks post-surgery. These ECs were studied to determine the systemic effects of BMP-2 treatment *in vivo* on the angiogenic potential of ECs and organ/tissue differences between lung and humeri ECs.

The ECs were characterized primarily based on their cell surface expression of CD31 [78] or of Tie2 as observed by expression of *TdTomato* following Cre recombination after mice were injected with tamoxifen (Supplemental Figs. 4, 14, and 15), confirming the phenotype of ECs isolated from the experimental animals. Furthermore, ECs were able to undergo functional tube formation, suggesting the tube forming ability was not affected by the expression of *TdTomato* (Supplemental Figs. 14 and 15).

Proliferation of ECs was previously shown to be enhanced in HFD animals and reduced in diabetes [79-81]. For instance, proliferation of ECs isolated from the epididymal white adipose tissue of HFD mice was increased compared to those isolated from LFD mice. On the other hand, proliferation of aortic ECs isolated from diabetic rabbits was severely decreased *in vitro*. Similarly, exposure of human umbilical vein endothelial cells (HUVECs) to high-glucose conditions resulted in impaired cell proliferation. Here, we found no significant difference in the proliferation of LECs or BMECs isolated from LFD versus HFD fed mice (Fig. 5). Furthermore, localized BMP-2 treatment *in vivo* 3 weeks prior to isolation of ECs did not affect the proliferation of lung or humeri derived ECs cultured *in vitro*. This may indicate that 3 weeks following local BMP-2 treatment, no significant systemic effects of BMP-2 treatment on EC proliferation exist.

In this study, tube formation in LECs and humeri BMECs was higher in the HFD group as compared to the LFD group for matched treatment groups (i.e. saline and

BMP-2 treated groups) (Fig. 6). A previous study reported an increase in tube formation of HUVEC cells treated with conditioned medium from epididymal fat tissue explants isolated from HFD mice [82]. Moreover, the study showed increased angiogenesis of solid tumors formed in HFD mice injected with CT26 colon cancer cells as compared to controls. Therefore, our results are consistent with these studies, showing HFD increases angiogenesis in ECs derived from both the lung and the humeri bone marrow.

On the other hand, we observed that BMP-2 treatment caused decreases in most of the angiogenic parameters examined for both LEC and humeri BMEC cultures, irrespective of diet, even though treatment was *in vivo* and 3 weeks prior to euthanasia of the mice, and the cells were cultured without further supplementation of BMP-2 (Fig. 6). We speculate this might be due to an inhibitory effect of matrix Gla protein (MGP) on BMP-2 associated angiogenesis, as MGP is known to be present in higher amounts in lungs and kidneys [83]. It may also be possible that angiogenesis is altered at a systemic level to allow more angiogenesis at or near the injury site in those that successfully heal (BMP-2) as compared to those that do not heal (saline).

Furthermore, we evaluated migration, an important characteristic of ECs [84] in BMECs to determine if localized treatment of BMP-2 at the time of surgery impacts the wound healing potential of BMECs 3 weeks later. Interestingly, humeri BMECs have more profound migration in HFD groups, particularly after BMP-2 treatment (Fig. 7). Of note, relative wound density is measured by normalizing the changes in cell density caused by proliferation and/or treatment effects. Thus, our conclusions are mainly based on wound confluence and wound width, which showed BMP-2 treatment enhanced migration potential in both LFD and HFD groups. Interestingly, tube formation was impaired with BMP-2 treatment irrespective of diet. Taken together, these data may suggest that BMP-2 treatment *in vivo* may promote *in vitro* EC migration at the expense of tube formation, especially in ECs isolated from BMP-2 treated, HFD-fed mice.

The role of CD31 in angiogenesis and migration is well known through a series of experiments that showed the inability of ECs grown on Matrigel to form tube-like structures due to inhibition by anti-CD31 antibody [85-88]. In our study, LECs showed that CD31 gene expression was significantly decreased in the HFD group treated with

BMP-2. This decrease might be related to a potential enrichment of MGP in lungs [83]. However, we did not observe a decrease in CD31 gene expression in the LFD group treated with BMP-2. Although not tested here, we speculate that the T2D-like phenotype might decrease the expression level of CD31 as MGP has been shown to be increased in human T2D patients' blood [89]. The fact that humeri BMECs also showed similar CD31 gene expression might indicate the influence of systemic factors that would need exploring in future studies to elucidate the mechanisms of action.

Although some studies demonstrate that FLT-1 can act as a negative regulator of angiogenesis, especially in the embryo [90-92], other studies demonstrate that FLT-1 is a positive regulator for angiogenesis and migration in ECs [93-95], suggesting its role in angiogenesis is likely context dependent. Here, we observed significant increases in FLT-1 mRNA expression in LECs as well as BMECs for LFD mice treated with BMP-2 compared to those treated with saline. However, a significant decrease in FLT-1 expression was observed in the HFD group treated with BMP-2 compared to saline treatment for LECs and BMECs. This might be due to aberrant VEGF signaling in the diabetic phenotype as has been previously suggested [96] and is consistent with the reduction in tube formation parameters reported here in HFD, BMP-2 treated mice compared to HFD, saline treated mice [96]. Along these lines, since VEGFR2/FLK1 is also an important receptor for VEGF, an examination of expression differences in the groups tested here could be important [97]. This is especially true in light of our findings that in the fracture callus, we observed that BMP-2 treatment, irrespective of diet, increased the vessel parameters (Fig. 4 and Supplemental Fig. 11). This may suggest that BMP-2 can increase sprouting *in vivo* regardless of diet. Notably, soluble VEGF regulates directionality of tip growth [98, 99]. *In vitro* our FLT-1 (VEGFR1) data show that BMP-2 treatment in LFD mice resulted in an ~7-fold increase in FLT-1 mRNA expression in humeri BMECs compared to BMECs from saline treated mice fed a LFD. However, BMECs from BMP-2 treatment of HFD mice had lower FLT-1 expression (~0.8 fold compared to LFD+Saline). Also, this decrease in FLT-1 expression is reflected in the increased migration and decreased wound width (Fig. 7). Taken together, this suggests that *in vitro*, BMP-2+LFD may be promoting an increase in more tip and/or stalk cells as has been reported by others [100], that are more directed and

able to form tubes *in vitro* from ECs isolated from LFD mice as compared to those isolated from HFD mice. While future studies are required to better dissect these possible mechanisms, examination of Notch-mediated signaling is likely important in this process.

ANGPT1 is a member of the angiopoietin family of growth factors and is the major agonist for the tyrosine kinase receptor Tek, which is found primarily on ECs [101]. We found that BMP-2 treatment did not alter the mRNA expression of ANGPT1 in LECs isolated from the LFD mice. However, we observed a significant decrease in the expression of ANGPT1 in LECs isolated from BMP-2 treated, HFD mice. The decrease in ANGPT1 in diabetic nephropathy has been previously reported [102]. Moreover, the combination of cartilage oligomeric matrix protein-angiopoietin 1 (COMP-Ang1), a synthetic variant of ANGPT1, and BMP-2 has been reported to heal craniofacial bone defects in C57BL/6 mice [103]. It is possible that the dose of BMP-2 used in our study was inadequate to increase the gene expression of ANGPT1 at a systemic level 3 weeks following treatment. Furthermore, it has been reported that streptozotocin injected mice showed decreased ANGPT1 mRNA expression in kidneys after 8 weeks. Thus, the time point at which we collected the tissues may be another factor contributing to the results observed in this study.

The role of ANGPT2 is context-dependent in ECs [104]. Endogenously, it acts as an antagonist to ANGPT1 in ECs [105]. The exogenous ANGPT2 activates Tie2 in ECs in the absence of ANGPT1 [106]. Interestingly, we observed in LECs that ANGPT2 mRNA expression was increased in LFD mice treated with BMP-2 as opposed to no change in expression for ANGPT1. However, there was a decrease in tube formation parameters in this group (LFD/BMP-2 vs. LFD/Saline) that lead us to conclude that ANGPT2 may act as an antagonist in this case. Further, serum ANGPT2 is a vital marker for T2D [107]. Due to the fact that we observed an antagonistic action of ANGPT2 in our study, it is possible that the decreased gene expression of ANGPT2 in the HFD group treated with BMP-2 might be due to protective effects of BMP-2 against the antagonist property of ANGPT2.

5. Conclusions

As fracture healing and angiogenesis are impaired in T2D, but BMP-2 is known to promote angiogenesis and fracture healing, here we sought to examine the impacts of BMP-2 treatment on fracture repair and angiogenesis with BMP-2 treatment in mice fed either a LFD or HFD. Our studies demonstrate that local administration of BMP-2 at the fracture site in a CSD model results in complete bone healing within 3 weeks for all HFD mice and 66.7% of LFD mice, whereas those treated with saline remain unhealed. We show that when LECs or BMECs are isolated from HFD mice, they have significantly improved tube formation properties compared to cells isolated from LFD mice. *In vivo*, differences based on diet are less pronounced. However, *in vivo*, BMP-2 treatment significantly increased vessel parameters at the fracture site, but not in the contralateral femur. This contrasts with the reduction in tube formation properties observed in ECs isolated from the lungs and bone marrow of these same mice but cultured in Matrigel. However, changes in FLT-1 expression along with increased migration of ECs derived from HFD fed mice treated with BMP-2 suggest that BMP-2 may be impacting tip and/or stalk cells and that directionality is differentially influenced by diet changes. Finally, contrary to the large body of evidence suggesting that fracture healing is impaired in those with T2D, we found that 3 weeks post-fracture, BMP-2 treatment promoted more robust fracture healing in HFD mice as compared to LFD mice. However, mechanical loading has been found to act synergistically with BMP signaling pathways and is able to amplify early, immediate steps of the Smad pathway [72]. Considering the heavier weights of the HFD mice, and thus the increased load placed on the injured limb, these findings, therefore, seem reasonable.

Importantly, these findings are only 3 weeks post-surgery and longer timepoints may demonstrate the deleterious impacts of HFD on the fracture repair process. Taken together, our data seem to suggest there may be benefits of using BMP-2 treatment for bone healing in patients with T2D, that they may experience a reduction in delayed/nonunion compared to those without T2D. However, in addition to the known side effects associated with BMP-2, additional possible side effects may be decreased vessel formation at some distal sites and increase adipogenesis within the fracture callus. While more work is needed to clarify these possibilities, continued investigations are critical, especially given the worldwide increased prevalence of diabetes and other

conditions related to abnormal angiogenesis (i.e., aging, hypertension, sedentarism). Especially, as use of BMP-2 may offer improvements to the treatment of fractures in T2D patients, which can have a significant impact on morbidity and quality of life for the present and future generations.

Author contributions

Study Design: FURB, UCD, JL, and MAK conceived the study. Study Conduct: FB, UCD, and CRV primarily conducted the experiments. Data analysis: FURB, UCD, CRV, NPT, ODA, CAS, SS, SKM, AJP, RUN, HLB, MKN, RJB, KAM, PJC, and JL contributed to the acquisition of data and the analysis of the data. These authors worked with JL and MAK to ensure the accuracy and integrity of the results. Data interpretation: All authors provided interpretation of various results. Drafting manuscript: FURB, SS, and MAK, with input from all co-authors, wrote the draft of the manuscript. Revising manuscript content/approving final version of manuscript: All authors revised the manuscript and approved the final content of the manuscript. JL and MAK take responsibility for the integrity of the data analysis.

Acknowledgements

This project was supported, in part, by the Cooperative Center of Excellence in Hematology (CCEH) Award, funded in part by NIH 1U54DK106846 (MAK, SS), NIH T32 DK007519 (UCD), NIH R01 AG060621 (MAK, JL, ODA), and National Science Foundation under (Grant No. 1618-408). In addition, the results of this work were supported with resources and the use of facilities at the Richard L. Roudebush VA Medical Center, Indianapolis, IN: VA Merit #BX003751 (MAK). We would also like to thank Dr. Carmella Evans-Molina and the Center for Diabetes & Metabolic Diseases Islet & Physiology Core (P30DK097512) at the Indiana University for conducting the GTT, ITT, and echoMRI measurements, the Angiogenesis Core (Indiana University Simon Cancer Center) for their assistance with running the wound migration assays, and the Histology and Histomorphometry Core (Indiana Center for Musculoskeletal Health) for this assistance with processing and staining of histological specimens. We would also like to thank Dr. Mervin C. Yoder, for kindly providing us with the Tie2-Cre^{ERT2}; tdTomato mice. Finally, the views expressed in this article are solely those of the authors and do not necessarily represent the official position or policy of any of the aforementioned agencies.

Key Resources Table

REAGENT or RESOURCES	SOURCE	IDENTIFIER
	Chemicals	
Tamoxifen	Sigma	T5648
Humilin R	Eli Lilly and Company	NDC 0002-8215-91 (HI-210)
Isoflurane	Patterson Veterinary	NDC 14043-704-5
Recombinant human bone morphogenetic protein-2 (rhBMP-2)	Medtronic Sofamor Danek Inc	7510903
Sodium chloride 0.9% in aqueous solution Normal saline solution, sterile	Aqualite Systems	NDC 0409-5168-38
Rodent Diet with 10kcal% fat (LOW FAT)	Research Diets	D12450H
Rodent Diet with 45kcal% fat HIGH FAT)	Research Diets	D12451
Eye Lubricant Major® LubriFresh™ P.M. 3.5 Gram Eye Ointment	Major Pharmaceuticals	904648838
Reagent Alcohol	Decon Laboratories, Inc	2705SG
Collagenase type 2	Worthington Biochemical Corporation	NC9522060
Dynabeads™ Biotin Binder	Thermo Fisher Scientific	11047
Endothelial Cell Growth Medium 2	PromoCell	C-22011
Endothelial Cell Medium	ScienCell	1001
Fetal bovine serum	ScienCell	0025
Endothelial Cell Growth Supplement	ScienCell	1052
Penicillin/Streptomycin Solution	ScienCell	0503
Penicillin-Streptomycin-Glutamine	Thermo Fisher Scientific	10378016
Fibronectin	Gibco	33016015
Richard-Allan Scientific™ Neutral Buffered Formalin (10%)	Thermo Fisher Scientific	5700TS
Phosphate-buffered saline	IBI Scientific	IB70166

Probumin® BSA Products	Sigma	82-002-4
DAPI (4',6-Diamidino- 2-Phenylindole, Dihydrochloride)	Thermo Fisher Scientific	D1306
Corning™ Matrigel™ Membrane Matrix	Corning®	354234
RNeasy Mini Kit	QIAGEN	74106
Transcriptor First Strand cDNA Synthesis Kit	Roche	4897030001
Power SYBR™ Green PCR Master Mix	Thermo Fisher Scientific	4367659
Corning® Collagen I, Rat Tail, 100mg	Corning®	354236
Povidone-Iodine Solution USP, 10% (w/v), 1% (w/v) Available Iodine, for Laboratory Use, Ricca Chemical	Purdue Products, LB	NDC 67618-150-01
Antibodies/Primers		
MS CD31 Biotin MAB, 0.5mg MEC 1	BD Biosciences	553371
Anti-CD31/PECAM-1, DyLight 488, Clone: MEC 7.46, antibody	Novus Biologicals™	NB1001642G
Materials		
3-0 polyglycolic acid suture	ETHICON	J215H
EZ clips non-sterile 7-mm	Braintree Scientific	RF7CS
Fisherbrand™ Sterile Cell Strainer (70 µm)	Thermo Fisher Scientific	22-363-548
Corning® BioCoat™ Collagen I-coated Plates	Corning®	356400
Corning® 96-well Clear Polystyrene Microplates	Corning®	3596
RCM6 Resorbable Collagen Membrane	ACE Surgical Supply Co., Inc.	509-3000
MS CD31 Biotin MAB, 0.5mg MEC 1	BD Biosciences	553371
Anti-CD31/PECAM-1, DyLight 488, Clone: MEC 7.46, antibody	Novus Biologicals™	NB1001642G
Instruments/Software		
EchoMRI™-100H Body Composition Analyzer	EchoMRI, LLC	100 H

200 Two Speed Rotary Tool	DREMEL	200 Series
Invitrogen DynaMag-2 Magnet	Thermo Fisher Scientific	12321D
EVOS® FL Cell Imaging System	Thermo Fisher Scientific	EVOS® FL
IncuCyte ZOOM® Live-Cell Analysis System	ESSEN BIOSCIENCE	ZOOM
IncuCyte™ Scratch Wound Cell Migration Software	ESSEN BIOSCIENCE	9600-0012
IncuCyte® Cell Migration Kit	ESSEN BIOSCIENCE	4493
CFX96 Touch Real-Time PCR Detection System	Bio-Rad	1855196

References

[1] J.S. Walsh, T. Vilaca, Obesity, Type 2 Diabetes and Bone in Adults, Calcif Tissue Int 100(5) (2017) 528-535.
[2] P. Vestergaard, Discrepancies in bone mineral density and fracture risk in patients with type 1 and type 2 diabetes--a meta-analysis, Osteoporos Int 18(4) (2007) 427-44.
[3] R. Dhaliwal, D. Cibula, C. Ghosh, R.S. Weinstock, A.M. Moses, Bone quality assessment in type 2 diabetes mellitus, Osteoporos Int 25(7) (2014) 1969-73.
[4] D.E. Sellmeyer, R. Civitelli, L.C. Hofbauer, S. Khosla, B. Lecka-Czernik, A.V. Schwartz, Skeletal Metabolism, Fracture Risk, and Fracture Outcomes in Type 1 and Type 2 Diabetes, Diabetes 65(7) (2016) 1757-66.
[5] V.V. Zhukouskaya, C. Eller-Vainicher, A. Gaudio, F. Privitera, E. Cairoli, F.M. Ulivieri, S. Palmieri, V. Morelli, V. Grancini, E. Orsi, B. Masserini, A.M. Spada, C.E. Fiore, I. Chiodini, The utility of lumbar spine trabecular bone score and femoral neck bone mineral density for identifying asymptomatic vertebral fractures in well-compensated type 2 diabetic patients, Osteoporos Int 27(1) (2016) 49-56.
[6] V. Sundararaghavan, M.M. Mazur, B. Evans, J. Liu, N.A. Ebraheim, Diabetes and bone health: latest evidence and clinical implications, Ther Adv Musculoskelet Dis 9(3) (2017) 67-74.
[7] F. Borgström, P. Sobocki, O. Ström, B. Jönsson, The societal burden of osteoporosis in Sweden, Bone 40(6) (2007) 1602-9.
[8] A.V. Schwartz, T.A. Hillier, D.E. Sellmeyer, H.E. Resnick, E. Gregg, K.E. Ensrud, P.J. Schreiner, K.L. Margolis, J.A. Cauley, M.C. Nevitt, D.M. Black, S.R. Cummings, Older women with diabetes have a higher risk of falls: a prospective study, Diabetes Care 25(10) (2002) 1749-54.
[9] N. Napoli, M. Chandran, D.D. Pierroz, B. Abrahamsen, A.V. Schwartz, S.L. Ferrari, I.O.F. Bone, G. Diabetes Working, Mechanisms of diabetes mellitus-induced bone fragility, Nat Rev Endocrinol 13(4) (2017) 208-219.
[10] R.T. Loder, The influence of diabetes mellitus on the healing of closed fractures, Clin Orthop Relat Res (232) (1988) 210-6.
[11] M. Janghorbani, D. Feskanich, W.C. Willett, F. Hu, Prospective study of diabetes and risk of hip fracture: the Nurses' Health Study, Diabetes Care 29(7) (2006) 1573-8.
[12] H. Jiao, E. Xiao, D.T. Graves, Diabetes and Its Effect on Bone and Fracture Healing, Curr Osteoporos Rep 13(5) (2015) 327-35.
[13] S. Henderson, I. Ibe, S. Cahill, Y.H. Chung, F.Y. Lee, Bone Quality and Fracture-Healing in Type-1 and Type-2 Diabetes Mellitus, J Bone Joint Surg Am 101(15) (2019) 1399-1410.
[14] R.E. Geuze, L.F. Theyse, D.H. Kempen, H.A. Hazewinkel, H.Y. Kraak, F.C. Oner, W.J. Dhert, J. Alblas, A differential effect of bone morphogenetic protein-2 and vascular endothelial growth factor release timing on osteogenesis at ectopic and orthotopic sites in a large-animal model, Tissue Eng Part A 18(19-20) (2012) 2052-62.
[15] A. Hernandez, R. Reyes, E. Sanchez, M. Rodriguez-Evora, A. Delgado, C. Evora, In vivo osteogenic response to different ratios of BMP-2 and VEGF released from a biodegradable porous system, J Biomed Mater Res A 100(9) (2012) 2382-91.
[16] C.I. Colnot, J.A. Helms, A molecular analysis of matrix remodeling and angiogenesis during long bone development, Mech Dev 100(2) (2001) 245-50.

[17] L.C. Gerstenfeld, D.M. Cullinane, G.L. Barnes, D.T. Graves, T.A. Einhorn, Fracture healing as a post-natal developmental process: molecular, spatial, and temporal aspects of its regulation, J Cell Biochem 88(5) (2003) 873-84.
[18] U. Saran, S. Gemini Piperni, S. Chatterjee, Role of angiogenesis in bone repair, Arch Biochem Biophys 561 (2014) 109-17.
[19] K.S. Chandrasekhar, H. Zhou, P. Zeng, D. Alge, W. Li, B.A. Finney, M.C. Yoder, J. Li, Blood vessel wall-derived endothelial colony-forming cells enhance fracture repair and bone regeneration, Calcif Tissue Int 89(5) (2011) 347-57.
[20] K.D. Hankenson, M. Dishowitz, C. Gray, M. Schenker, Angiogenesis in bone regeneration, Injury 42(6) (2011) 556-561.
[21] L. Lamalice, F. Le Boeuf, J. Huot, Endothelial cell migration during angiogenesis, Circ Res 100(6) (2007) 782-94.
[22] R. Marcu, Y.J. Choi, J. Xue, C.L. Fortin, Y. Wang, R.J. Nagao, J. Xu, J.W. MacDonald, T.K. Bammler, C.E. Murry, K. Muczynski, K.R. Stevens, J. Himmelfarb, S.M. Schwartz, Y. Zheng, Human Organ-Specific Endothelial Cell Heterogeneity, iScience 4 (2018) 20-35.
[23] H.P. Gerber, N. Ferrara, Angiogenesis and bone growth, Trends Cardiovasc Med 10(5) (2000) 223-8.
[24] J. Dai, A.B. Rabie, VEGF: an essential mediator of both angiogenesis and endochondral ossification, J Dent Res 86(10) (2007) 937-50.
[25] I. Eshkar-Oren, S.V. Viukov, S. Salameh, S. Krief, C.D. Oh, H. Akiyama, H.P. Gerber, N. Ferrara, E. Zelzer, The forming limb skeleton serves as a signaling center for limb vasculature patterning via regulation of Vegf, Development 136(8) (2009) 1263-72.
[26] S.K. Ramasamy, A.P. Kusumbe, L. Wang, R.H. Adams, Endothelial Notch activity promotes angiogenesis and osteogenesis in bone, Nature 507(7492) (2014) 376-380.
[27] A.P. Kusumbe, S.K. Ramasamy, R.H. Adams, Coupling of angiogenesis and osteogenesis by a specific vessel subtype in bone, Nature 507(7492) (2014) 323-328.
[28] A. Grosso, M.G. Burger, A. Lunger, D.J. Schaefer, A. Banfi, N. Di Maggio, It Takes Two to Tango: Coupling of Angiogenesis and Osteogenesis for Bone Regeneration, Front Bioeng Biotechnol 5 (2017) 68.
[29] F. Ugarte, E.C. Forsberg, Haematopoietic stem cell niches: new insights inspire new questions, EMBO J 32(19) (2013) 2535-47.
[30] B. Beamer, C. Hettrich, J. Lane, Vascular endothelial growth factor: an essential component of angiogenesis and fracture healing, Hss j 6(1) (2010) 85-94.
[31] C. Carulli, M. Innocenti, M.L. Brandi, Bone vascularization in normal and disease conditions, Front Endocrinol (Lausanne) 4 (2013) 106.
[32] A.K. Gosain, L. Song, P. Yu, B.J. Mehrara, C.Y. Maeda, L.I. Gold, M.T. Longaker, Osteogenesis in cranial defects: reassessment of the concept of critical size and the expression of TGF-beta isoforms, Plast Reconstr Surg 106(2) (2000) 360-71; discussion 372.
[33] C.L. Hochstetler, Y. Feng, M. Sacma, A.K. Davis, M. Rao, C.Y. Kuan, L.R. You, H. Geiger, Y. Zheng, KRas(G12D) expression in the bone marrow vascular niche affects hematopoiesis with inflammatory signals, Exp Hematol 79 (2019) 3-15.e4.
[34] T.M. Chu, S.J. Warden, C.H. Turner, R.L. Stewart, Segmental bone regeneration using a load-bearing biodegradable carrier of bone morphogenetic protein-2, Biomaterials 28(3) (2007) 459-67.

[35] D.B. Whelan, M. Bhandari, D. Stephen, H. Kreder, M.D. McKee, R. Zdero, E.H. Schemitsch, Development of the radiographic union score for tibial fractures for the assessment of tibial fracture healing after intramedullary fixation, J Trauma 68(3) (2010) 629-32.
[36] P. Childress, A. Brinker, C.S. Gong, J. Harris, D.J. Olivos, 3rd, J.D. Rytlewski, D.C. Scofield, S.Y. Choi, Y. Shirazi-Fard, T.O. McKinley, T.G. Chu, C.L. Conley, N. Chakraborty, R. Hammamieh, M.A. Kacena, Forces associated with launch into space do not impact bone fracture healing, Life Sci Space Res (Amst) 16 (2018) 52-62.
[37] M.E. Cooke, A.I. Hussein, K.E. Lybrand, A. Wulff, E. Simmons, J.H. Choi, J. Litrenta, W.M. Ricci, J.W. Nascone, R.V. O'Toole, E.F. Morgan, L.C. Gerstenfeld, P. Tornetta, 3rd, Correlation between RUST assessments of fracture healing to structural and biomechanical properties, J Orthop Res 36(3) (2018) 945-953.
[38] C.D. Collier, B.S. Hausman, S.H. Zulqadar, E.S. Din, J.M. Anderson, O. Akkus, E.M. Greenfield, Characterization of a reproducible model of fracture healing in mice using an open femoral osteotomy, Bone Rep 12 (2020) 100250.
[39] P.L. Mulcrone, J.P. Campbell, L. Clement-Demange, A.L. Anbinder, A.R. Merkel, R.A. Brekken, J.A. Sterling, F. Elefteriou, Skeletal Colonization by Breast Cancer Cells Is Stimulated by an Osteoblast and beta2AR-Dependent Neo-Angiogenic Switch, J Bone Miner Res 32(7) (2017) 1442-1454.
[40] J. Wang, N. Niu, S. Xu, Z.G. Jin, A simple protocol for isolating mouse lung endothelial cells, Sci Rep 9(1) (2019) 1458.
[41] C.T. Rueden, J. Schindelin, M.C. Hiner, B.E. DeZonia, A.E. Walter, E.T. Arena, K.W. Eliceiri, ImageJ2: ImageJ for the next generation of scientific image data, BMC Bioinformatics 18(1) (2017) 529.
[42] H.B. Pearson, D.E. Mason, C.D. Kegelman, L. Zhao, J.H. Dawahare, M.A. Kacena, J.D. Boerckel, Effects of Bone Morphogenetic Protein-2 on Neovascularization During Large Bone Defect Regeneration, Tissue Eng Part A (2019).
[43] J. Schindelin, I. Arganda-Carreras, E. Frise, V. Kaynig, M. Longair, T. Pietzsch, S. Preibisch, C. Rueden, S. Saalfeld, B. Schmid, J.Y. Tinevez, D.J. White, V. Hartenstein, K. Eliceiri, P. Tomancak, A. Cardona, Fiji: an open-source platform for biological-image analysis, Nat Methods 9(7) (2012) 676-82.
[44] H. Sekiguchi, M. Ii, K. Jujo, A. Yokoyama, N. Hagiwara, T. Asahara, Improved culture-based isolation of differentiating endothelial progenitor cells from mouse bone marrow mononuclear cells, PLoS One 6(12) (2011) e28639.
[45] P.L. Mulcrone, J.P. Campbell, L. Clément-Demange, A.L. Anbinder, A.R. Merkel, R.A. Brekken, J.A. Sterling, F. Elefteriou, Skeletal Colonization by Breast Cancer Cells Is Stimulated by an Osteoblast and β2AR-Dependent Neo-Angiogenic Switch, J Bone Miner Res 32(7) (2017) 1442-1454.
[46] L. Clément-Demange, P.L. Mulcrone, T.Q. Tabarestani, J.A. Sterling, F. Elefteriou, β2ARs stimulation in osteoblasts promotes breast cancer cell adhesion to bone marrow endothelial cells in an IL-1β and selectin-dependent manner, J Bone Oncol 13 (2018) 1-10.
[47] M. Janghorbani, R.M. Van Dam, W.C. Willett, F.B. Hu, Systematic review of type 1 and type 2 diabetes mellitus and risk of fracture, Am J Epidemiol 166(5) (2007) 495-505.

[48] N.B. Khazai, G.R. Beck, Jr., G.E. Umpierrez, Diabetes and fractures: an overshadowed association, Curr Opin Endocrinol Diabetes Obes 16(6) (2009) 435-45.
[49] A.V. Schwartz, E. Vittinghoff, D.C. Bauer, T.A. Hillier, E.S. Strotmeyer, K.E. Ensrud, M.G. Donaldson, J.A. Cauley, T.B. Harris, A. Koster, C.R. Womack, L. Palermo, D.M. Black, Association of BMD and FRAX score with risk of fracture in older adults with type 2 diabetes, Jama 305(21) (2011) 2184-92.
[50] E.S. Strotmeyer, J.A. Cauley, Diabetes mellitus, bone mineral density, and fracture risk, Curr Opin Endocrinol Diabetes Obes 14(6) (2007) 429-35.
[51] D.T. Graves, J. Alblowi, D.N. Paglia, J.P. O'Connor, S. Lin, Impact of Diabetes on Fracture Healing, Journal of Experimental & Clinical Medicine 3(1) (2011) 3-8.
[52] H. Heath, L.J. Melton, C.-P. Chu, Diabetes Mellitus and Risk of Skeletal Fracture, New England Journal of Medicine 303(10) (1980) 567-570.
[53] M. Sosa, P. Saavedra, E. Jódar, C. Lozano-Tonkin, J.M. Quesada, A. Torrijos, R. Pérez-Cano, X. Nogués, M. Díaz-Curiel, M.J. Moro, C. Gómez, J. Mosquera, J. Alegre, J. Olmos, M. Muñoz-Torres, N. Guañabens, J. Del Pino, F. Hawkins, Bone mineral density and risk of fractures in aging, obese post-menopausal women with type 2 diabetes. The GIUMO Study, Aging Clin Exp Res 21(1) (2009) 27-32.
[54] L.M. Giangregorio, W.D. Leslie, L.M. Lix, H. Johansson, A. Oden, E. McCloskey, J.A. Kanis, FRAX underestimates fracture risk in patients with diabetes, J Bone Miner Res 27(2) (2012) 301-8.
[55] A.J. Kline, G.S. Gruen, H.C. Pape, I.S. Tarkin, J.J. Irrgang, D.K. Wukich, Early complications following the operative treatment of pilon fractures with and without diabetes, Foot Ankle Int 30(11) (2009) 1042-7.
[56] F.C. Senel, G.S. Jessen, M.D. Melo, G. Obeid, Infection following treatment of mandible fractures: the role of immunosuppression and polysubstance abuse, Oral Surg Oral Med Oral Pathol Oral Radiol Endod 103(1) (2007) 38-42.
[57] S. Adami, Bone health in diabetes: considerations for clinical management, Curr Med Res Opin 25(5) (2009) 1057-72.
[58] R.K. Hernandez, T.P. Do, C.W. Critchlow, R.E. Dent, S.S. Jick, Patient-related risk factors for fracture-healing complications in the United Kingdom General Practice Research Database, Acta Orthop 83(6) (2012) 653-60.
[59] C.Y. Wang, J.K. Liao, A mouse model of diet-induced obesity and insulin resistance, Methods Mol Biol 821 (2012) 421-33.
[60] C. Nagy, E. Einwallner, Study of In Vivo Glucose Metabolism in High-fat Diet-fed Mice Using Oral Glucose Tolerance Test (OGTT) and Insulin Tolerance Test (ITT), J Vis Exp (131) (2018).
[61] A.J. King, The use of animal models in diabetes research, Br J Pharmacol 166(3) (2012) 877-94.
[62] O. Jeon, J.W. Rhie, I.K. Kwon, J.H. Kim, B.S. Kim, S.H. Lee, In vivo bone formation following transplantation of human adipose-derived stromal cells that are not differentiated osteogenically, Tissue Eng Part A 14(8) (2008) 1285-94.
[63] J.C. Rivera, C.A. Strohbach, J.C. Wenke, C.R. Rathbone, Beyond osteogenesis: an in vitro comparison of the potentials of six bone morphogenetic proteins, Front Pharmacol 4 (2013) 125.

[64] A. Kolk, T. Tischer, C. Koch, S. Vogt, B. Haller, R. Smeets, K. Kreutzer, C. Plank, O. Bissinger, A novel nonviral gene delivery tool of BMP-2 for the reconstitution of critical-size bone defects in rats, J Biomed Mater Res A 104(10) (2016) 2441-55.
[65] D. Suarez-Gonzalez, J.S. Lee, A. Diggs, Y. Lu, B. Nemke, M. Markel, S.J. Hollister, W.L. Murphy, Controlled multiple growth factor delivery from bone tissue engineering scaffolds via designed affinity, Tissue Eng Part A 20(15-16) (2014) 2077-87.
[66] M.S. Bae, J.Y. Ohe, J.B. Lee, D.N. Heo, W. Byun, H. Bae, Y.D. Kwon, I.K. Kwon, Photo-cured hyaluronic acid-based hydrogels containing growth and differentiation factor 5 (GDF-5) for bone tissue regeneration, Bone 59 (2014) 189-98.
[67] P.M. Arrabal, R. Visser, L. Santos-Ruiz, J. Becerra, M. Cifuentes, Osteogenic molecules for clinical applications: improving the BMP-collagen system, Biol Res 46(4) (2013) 421-9.
[68] A.F. Kamal, O.S.H. Siahaan, J. Fiolin, Various Dosages of BMP-2 for Management of Massive Bone Defect in Sprague Dawley Rat, Arch Bone Jt Surg 7(6) (2019) 498-505.
[69] X. Wei, S. Egawa, R. Matsumoto, H. Yasuda, K. Hirai, T. Yoshii, A. Okawa, T. Nakajima, S. Sotome, Augmentation of fracture healing by hydroxyapatite/collagen paste and bone morphogenetic protein-2 evaluated using a rat femur osteotomy model, Journal of Orthopaedic Research 36(1) (2018) 129-137.
[70] C.R. Rueff-Barroso, J. Milagres D Fau - do Valle, G. do Valle J Fau - Casimiro-Lopes, J.F. Casimiro-Lopes G Fau - Nogueira-Neto, J.F.C. Nogueira-Neto Jf Fau - Zanier, L.C. Zanier Jf Fau - Porto, L.C. Porto, Bone healing in rats submitted to weight-bearing and non-weight-bearing exercises, (1643-3750 (Electronic)).
[71] I.B. Houben, M. Raaben, M. Van Basten Batenburg, T.J. Blokhuis, Delay in weight bearing in surgically treated tibial shaft fractures is associated with impaired healing: a cohort analysis of 166 tibial fractures, Eur J Orthop Surg Traumatol 28(7) (2018) 1429-1436.
[72] J. Kopf, A. Petersen, G.N. Duda, P. Knaus, BMP2 and mechanical loading cooperatively regulate immediate early signalling events in the BMP pathway, BMC Biology 10(1) (2012) 37.
[73] F. Pirih, J. Lu, F. Ye, O. Bezouglaia, E. Atti, M.G. Ascenzi, S. Tetradis, L. Demer, T. Aghaloo, Y. Tintut, Adverse effects of hyperlipidemia on bone regeneration and strength, J Bone Miner Res 27(2) (2012) 309-18.
[74] M.L. Brown, K. Yukata, C.W. Farnsworth, D.G. Chen, H. Awad, M.J. Hilton, R.J. O'Keefe, L. Xing, R.A. Mooney, M.J. Zuscik, Delayed fracture healing and increased callus adiposity in a C57BL/6J murine model of obesity-associated type 2 diabetes mellitus, PLoS One 9(6) (2014) e99656.
[75] T. Histing, A. Andonyan, M. Klein, C. Scheuer, D. Stenger, J.H. Holstein, N.T. Veith, T. Pohlemann, M.D. Menger, Obesity does not affect the healing of femur fractures in mice, Injury 47(7) (2016) 1435-44.
[76] M. Beederman, J.D. Lamplot, G. Nan, J. Wang, X. Liu, L. Yin, R. Li, W. Shui, H. Zhang, S.H. Kim, W. Zhang, J. Zhang, Y. Kong, S. Denduluri, M.R. Rogers, A. Pratt, R.C. Haydon, H.H. Luu, J. Angeles, L.L. Shi, T.-C. He, BMP signaling in mesenchymal stem cell differentiation and bone formation, J Biomed Sci Eng 6(8A) (2013) 32-52.
[77] S.Y. Lee, J.H. Lee, J.Y. Kim, Y.C. Bae, K.T. Suh, J.S. Jung, BMP2 increases adipogenic differentiation in the presence of dexamethasone, which is inhibited by the

treatment of TNF-α in human adipose tissue-derived stromal cells, Cell Physiol Biochem 34(4) (2014) 1339-50.
[78] L.A. Oosterhoff, H.S. Kruitwagen, M.E. van Wolferen, B.W.M. van Balkom, M. Mokry, N. Lansu, N.A.M. van den Dungen, L.C. Penning, T.C.F. Spanjersberg, J.W. de Graaf, T. Veenendaal, F. Zomerdijk, J.O. Fledderus, B. Spee, F.G. van Steenbeek, Characterization of Endothelial and Smooth Muscle Cells From Different Canine Vessels, Front Physiol 10 (2019) 101.
[79] S.M. Santilli, V.D. Fiegel, D.E. Aldridge, D.R. Knighton, The effect of diabetes on the proliferation of aortic endothelial cells, Ann Vasc Surg 6(6) (1992) 503-10.
[80] X. Chen, M.N. Duong, P.J. Psaltis, C.A. Bursill, S.J. Nicholls, High-density lipoproteins attenuate high glucose-impaired endothelial cell signaling and functions: potential implications for improved vascular repair in diabetes, Cardiovasc Diabetol 16(1) (2017) 121.
[81] K. Adamcova, O. Horakova, K. Bardova, P. Janovska, M. Brezinova, O. Kuda, M. Rossmeisl, J. Kopecky, Reduced Number of Adipose Lineage and Endothelial Cells in Epididymal fat in Response to Omega-3 PUFA in Mice Fed High-Fat Diet, Mar Drugs 16(12) (2018).
[82] H. Park, M. Kim, G.T. Kwon, D.Y. Lim, R. Yu, M.K. Sung, K.W. Lee, J.W. Daily, 3rd, J.H. Park, A high-fat diet increases angiogenesis, solid tumor growth, and lung metastasis of CT26 colon cancer cells in obesity-resistant BALB/c mice, Mol Carcinog 51(11) (2012) 869-80.
[83] Y. Yao, A.D. Watson, S. Ji, K.I. Bostrom, Heat shock protein 70 enhances vascular bone morphogenetic protein-4 signaling by binding matrix Gla protein, Circ Res 105(6) (2009) 575-84.
[84] S. Guo, J. Lok, Y. Liu, K. Hayakawa, W. Leung, C. Xing, X. Ji, E.H. Lo, Assays to examine endothelial cell migration, tube formation, and gene expression profiles, Methods Mol Biol 1135 (2014) 393-402.
[85] H.M. DeLisser, M. Christofidou-Solomidou, R.M. Strieter, M.D. Burdick, C.S. Robinson, R.S. Wexler, J.S. Kerr, C. Garlanda, J.R. Merwin, J.A. Madri, S.M. Albelda, Involvement of endothelial PECAM-1/CD31 in angiogenesis, Am J Pathol 151(3) (1997) 671-7.
[86] N. Sheibani, P.J. Newman, W.A. Frazier, Thrombospondin-1, a natural inhibitor of angiogenesis, regulates platelet-endothelial cell adhesion molecule-1 expression and endothelial cell morphogenesis, Mol Biol Cell 8(7) (1997) 1329-41.
[87] T. Matsumura, K. Wolff, P. Petzelbauer, Endothelial cell tube formation depends on cadherin 5 and CD31 interactions with filamentous actin, J Immunol 158(7) (1997) 3408-16.
[88] S. Yang, J. Graham, J.W. Kahn, E.A. Schwartz, M.E. Gerritsen, Functional roles for PECAM-1 (CD31) and VE-cadherin (CD144) in tube assembly and lumen formation in three-dimensional collagen gels, Am J Pathol 155(3) (1999) 887-95.
[89] S.B. Thomsen, C.N. Rathcke, B. Zerahn, H. Vestergaard, Increased levels of the calcification marker matrix Gla Protein and the inflammatory markers YKL-40 and CRP in patients with type 2 diabetes and ischemic heart disease, Cardiovasc Diabetol 9 (2010) 86.

[90] S. Hiratsuka, Y. Maru, A. Okada, M. Seiki, T. Noda, M. Shibuya, Involvement of Flt-1 tyrosine kinase (vascular endothelial growth factor receptor-1) in pathological angiogenesis, Cancer Res 61(3) (2001) 1207-13.
[91] M. Shibuya, Vascular endothelial growth factor receptor-1 (VEGFR-1/Flt-1): a dual regulator for angiogenesis, Angiogenesis 9(4) (2006) 225-230.
[92] J. Krueger, D. Liu, K. Scholz, A. Zimmer, Y. Shi, C. Klein, A. Siekmann, S. Schulte-Merker, M. Cudmore, A. Ahmed, F. le Noble, Flt1 acts as a negative regulator of tip cell formation and branching morphogenesis in the zebrafish embryo, Development 138(10) (2011) 2111-20.
[93] H.P. Gerber, F. Condorelli, J. Park, N. Ferrara, Differential transcriptional regulation of the two vascular endothelial growth factor receptor genes. Flt-1, but not Flk-1/KDR, is up-regulated by hypoxia, J Biol Chem 272(38) (1997) 23659-67.
[94] B. Olofsson, E. Korpelainen, M.S. Pepper, S.J. Mandriota, K. Aase, V. Kumar, Y. Gunji, M.M. Jeltsch, M. Shibuya, K. Alitalo, U. Eriksson, Vascular endothelial growth factor B (VEGF-B) binds to VEGF receptor-1 and regulates plasminogen activator activity in endothelial cells, Proc Natl Acad Sci U S A 95(20) (1998) 11709-14.
[95] H.K. Lee, S.K. Chauhan, E. Kay, R. Dana, Flt-1 regulates vascular endothelial cell migration via a protein tyrosine kinase-7-dependent pathway, Blood 117(21) (2011) 5762-71.
[96] J.C. Chappell, K.P. Mouillesseaux, V.L. Bautch, Flt-1 (vascular endothelial growth factor receptor-1) is essential for the vascular endothelial growth factor-Notch feedback loop during angiogenesis, Arterioscler Thromb Vasc Biol 33(8) (2013) 1952-9.
[97] O. Katoh, H. Tauchi, K. Kawaishi, A. Kimura, Y. Satow, Expression of the vascular endothelial growth factor (VEGF) receptor gene, KDR, in hematopoietic cells and inhibitory effect of VEGF on apoptotic cell death caused by ionizing radiation, Cancer Res 55(23) (1995) 5687-92.
[98] H. Gerhardt, M. Golding, M. Fruttiger, C. Ruhrberg, A. Lundkvist, A. Abramsson, M. Jeltsch, C. Mitchell, K. Alitalo, D. Shima, C. Betsholtz, VEGF guides angiogenic sprouting utilizing endothelial tip cell filopodia, J Cell Biol 161(6) (2003) 1163-77.
[99] R. Blanco, H. Gerhardt, VEGF and Notch in tip and stalk cell selection, Cold Spring Harb Perspect Med 3(1) (2013) a006569.
[100] A. Benn, C. Hiepen, M. Osterland, C. Schütte, A. Zwijsen, P. Knaus, Role of bone morphogenetic proteins in sprouting angiogenesis: differential BMP receptor-dependent signaling pathways balance stalk vs. tip cell competence, Faseb j 31(11) (2017) 4720-4733.
[101] M. Jeansson, A. Gawlik, G. Anderson, C. Li, D. Kerjaschki, M. Henkelman, S.E. Quaggin, Angiopoietin-1 is essential in mouse vasculature during development and in response to injury, J Clin Invest 121(6) (2011) 2278-89.
[102] L. Gnudi, Angiopoietins and diabetic nephropathy, Diabetologia 59(8) (2016) 1616-20.
[103] H. Choi, B.C. Jeong, S.W. Hur, J.W. Kim, K.B. Lee, J.T. Koh, The Angiopoietin-1 Variant COMP-Ang1 Enhances BMP2-Induced Bone Regeneration with Recruiting Pericytes in Critical Sized Calvarial Defects, PLoS One 10(10) (2015) e0140502.
[104] G. Thurston, C. Daly, The complex role of angiopoietin-2 in the angiopoietin-tie signaling pathway, Cold Spring Harb Perspect Med 2(9) (2012) a006550.

[105] P.C. Maisonpierre, C. Suri, P.F. Jones, S. Bartunkova, S.J. Wiegand, C. Radziejewski, D. Compton, J. McClain, T.H. Aldrich, N. Papadopoulos, T.J. Daly, S. Davis, T.N. Sato, G.D. Yancopoulos, Angiopoietin-2, a natural antagonist for Tie2 that disrupts in vivo angiogenesis, Science 277(5322) (1997) 55-60.
[106] H.T. Yuan, E.V. Khankin, S.A. Karumanchi, S.M. Parikh, Angiopoietin 2 is a partial agonist/antagonist of Tie2 signaling in the endothelium, Mol Cell Biol 29(8) (2009) 2011-22.
[107] K. Siddiqui, S.S. Joy, S.S. Nawaz, Serum Angiopoietin-2 levels as a marker in type 2 diabetes mellitus complications, International Journal of Diabetes in Developing Countries 39(2) (2019) 387-393.

Author contributions

Study Design: FURB, UCD, JL, and MAK conceived the study. Study Conduct: FB, UCD, and CRV primarily conducted the experiments. Data analysis: FURB, UCD, CRV, NPT, ODA, CAS, SS, SKM, AJP, RUN, HLB, MKN, RJB, KAM, PJC, and JL contributed to the acquisition of data and the analysis of the data. These authors worked with JL and MAK to ensure the accuracy and integrity of the results. Data interpretation: All authors provided interpretation of various results. Drafting manuscript: FURB, SS, and MAK, with input from all co-authors, wrote the draft of the manuscript. Revising manuscript content/approving final version of manuscript: All authors revised the manuscript and approved the final content of the manuscript. JL and MAK take responsibility for the integrity of the data analysis.

Highlights

- Mice fed HFD for 12 weeks acquired a T2D-like metabolic phenotype
- BMP-2 treatment enhanced fracture healing in HFD mice 3 weeks post-surgery
- BMP-2 promotes vessel and adipocyte formation in the fracture callus
- ECs isolated from lungs and bone marrow of HFD mice have enhanced tube formation
- BMP-2 treatment *in vivo* 3 weeks prior to EC isolation inhibits tube formation *in vitro*